AFIT/GE/ENG/91D-43

Design and Testing of a Lightweight, Planar Microwave Lens

THESIS

Paul Michael Proudfoot
Captain, USAF

AFIT/GE/ENG/91D-43

DISCLAIMER NOTICE

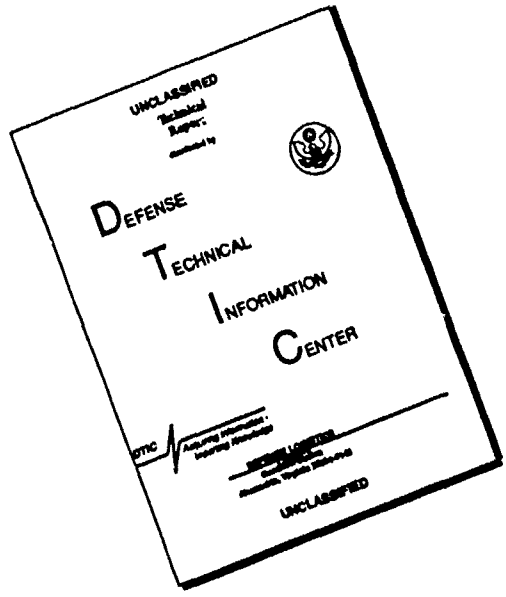

THIS DOCUMENT IS BEST QUALITY AVAILABLE. THE COPY FURNISHED TO DTIC CONTAINED A SIGNIFICANT NUMBER OF PAGES WHICH DO NOT REPRODUCE LEGIBLY.

REPORT DOCUMENTATION PAGE

Form Approved
OMB No 0704-0188

1. AGENCY USE ONLY (Leave blank)	2. REPORT DATE	3. REPORT TYPE AND DATES COVERED
	December 1991	Master's Thesis

4. TITLE AND SUBTITLE

Design and Testing of a Lightweight, Planar Microwave Lens

5. FUNDING NUMBERS

6. AUTHOR(S)

Paul M. Proudfoot, Captain, USAF

7. PERFORMING ORGANIZATION NAME(S) AND ADDRESS(ES)

Air Force Institute of Technology
WPAFB, OH 45433-6583

8. PERFORMING ORGANIZATION REPORT NUMBER

AFIT/GE/ENG/91D-43

9. SPONSORING/MONITORING AGENCY NAME(S) AND ADDRESS(ES)

Rome Laboratory
EEA
Hanscom AFB, MA 01731

10. SPONSORING/MONITORING AGENCY REPORT NUMBER

11. SUPPLEMENTARY NOTES

12a. DISTRIBUTION/AVAILABILITY STATEMENT

Approved for public release; distribution unlimited

12b. DISTRIBUTION CODE

13. ABSTRACT (Maximum 200 words)

This thesis documents the design, fabrication, and testing of a lightweight, planar microwave lens. The lens consists of two planar arrays of lightweight printed circuit antennas interconnected by microstrip lines whose length varies as a function of position on the lens. Microwave energy is coupled from one face of the lens to the other by means of a slot etched in the ground plane. At 8.0 GHz the lens is ten wavelengths across, is less than 1/8 inch thick, and weighs less than 4 pounds. The lens can scan a beam over a +/- 30 degree region in both the azimuth and elevation planes. The overall lens efficiency is 56 percent, a 25 percent increase over previous planar lens designs.

14. SUBJECT TERMS

Microwave Lens, Lens Antenna

15. NUMBER OF PAGES **79**

16. PRICE CODE

17. SECURITY CLASSIFICATION OF REPORT	18. SECURITY CLASSIFICATION OF THIS PAGE	19. SECURITY CLASSIFICATION OF ABSTRACT	20. LIMITATION OF ABSTRACT
Unclassified	**Unclassified**	**Unclassified**	**UL**

AFIT/GE/ENG/91D-43

Design and Testing of a Lightweight, Planar Microwave Lens

THESIS

Presented to the Faculty of the School of Engineering

of the Air Force Institute of Technology

Air University

In Partial Fulfillment of the

Requirements for the Degree of

Master of Science (Electrical Engineering)

Paul Michael Proudfoot, B.S.

Captain, USAF

December, 1991

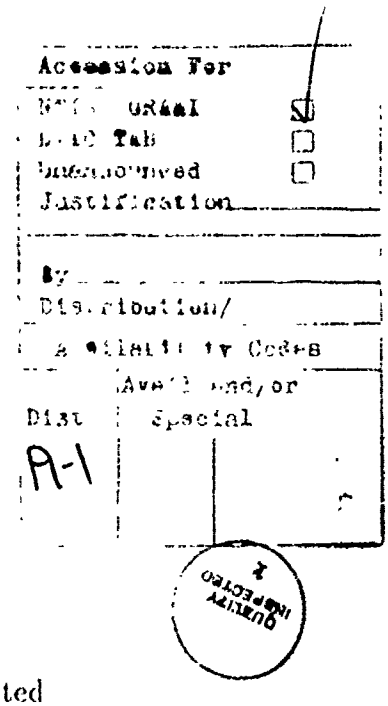

Table of Contents

List of Figures

List of Tables

Abstract

This thesis documents the design, fabrication, and testing of a planar microwave lens. The lens consists of two planar arrays of light-weight printed circuit antennas interconnected by microstrip lines whose length varies as a function of position on the lens. Microwave energy is coupled from one face of the lens to the other by means of a slot etched in the ground plane. At 8.0 GHz the lens is ten wavelengths across, is less than 1/8 inch thick, and weighs less than 4 pounds. The lens can scan a beam over a ± 30 degree region in both the azimuth and elevation planes. The overall lens efficiency is 56 percent, a 25 percent increase over previous planar lens designs.

Design and Testing of a Lightweight, Planar Microwave Lens

I. Introduction

1.1 General Issue

Microwave lenses are used in applications where high gain and/or wide scanning capabilities are required. The Department of Defense is currently using one or more microwave lenses in several of its satellite systems. These systems include ACTS, MILSTAR and DSCS. One disadvantage in using a microwave lens in a space application is its extreme weight. A microwave lens can weigh on the order of 100 pounds or more. Methods which attempt to reduce lens weight, such as zoning [1], also introduce undesirable effects. These effects include increased sidelobe levels due to shadowing and reduced bandwidth, hence system performance is degraded.

1.2 Problem Statement

A reduction in weight of a microwave lens is required without degradation of system performance.

1.3 Research Objective

This thesis covers the design and testing of a lightweight planar microwave lens. A previous lens [2] designed by McGrath is the foundation for this effort. Improvements to the McGrath design are made to increase overall lens efficiency. After the lens was designed and fabricated, the lens was tested for both radiation characteristics and for overall lens efficiency. An attempt was made to quantify all loss mechanisms encountered in the lens, however, the primary emphasis was focused on overall lens efficiency.

1.4 Approach

A planar constrained lens approach is used for the lens architecture. Architectures of this type require both aperture- and feed-side radiating elements and

connecting transmission lines. Lightweight microstrip patch antennas are used as both the aperture- and feed-side radiating elements. Varying lengths of microstrip transmission lines are then used to feed the patch antennas. A critical element to the success of this thesis hinged on finding an efficient means of transmitting energy from one face of the lens to the other. Therefore, design and testing of the lens was accomplished in two steps. First, a prototype feedthrough was designed and then tested for insertion loss. Once an efficient feedthrough design was found, the lens was then designed and tested. This two-step procedure eliminated much of the risk in trying to design a lens with a high overall efficiency.

1.5 Limitations

The design phase of this effort is limited to using existing models that appear in literature for the characterization of microstrip transmission lines, patch antennas and feedthroughs. An exact model for the feedthrough design does not appear in the literature and an approximate model is used to establish a base line design. Final feedthrough design is based on prototype tests results.

1.6 Materials and Equipment

Dielectric material used for lens fabrication was supplied by Rome Laboratory. Lens fabrication was also accomplished at Rome Laboratory through an in-place service contract with Wentworth Industries, Newton, Massachusetts.

Testing of the microwave lens required an antenna measurement range of 45 feet or more, with a rotating pedestal capable of handling weights of approximately 50 pounds. The Rome Laboratory antenna measurement facility at Ipswich, Massachusetts was used for lens testing.

Prototype feedthrough testing was accomplished at AFIT using an HP 8510 Automatic Network Analyzer located in Building 194.

1.7 Overview of the Thesis

Chapter 2 of the thesis is a literature review. The literature review provides background information on the topic of planar microwave lenses. Also, a brief history of the constrained lens is presented. Chapter 3 covers the design, fabrication and testing of the prototype feedthroughs. Chapter 4 describes the design, fabrication

and testing of the lens. Chapter 5 summarizes the work accomplished, provides conclusions, and presents recommendations for future research.

II. Literature Review

2.1 Introduction

This chapter is intended to survey the topic of planar microwave lenses and identify what others have done in this area. While documentation on the topic of lenses in general is broad and covers many frequency bands, documentation on the topic of lenses at microwave frequencies is less abundant. A planar lens further restricts the topic, since only a few planar lenses have ever been documented. These few papers will be the subject of this chapter and will form the starting point for this research. The chapter is divided into two parts. First, some background material on the microwave lens, its importance, and applications will be presented. Second, previous work on the planar microwave lens will be discussed as well as the problems encountered and conclusions of the work.

2.2 Background

A lens in either the optical or the microwave frequency spectrum would work, in principle, the same way. In each case, rays that travel from some wavefront, through the lens, to the focal point, must travel an equal path length. Most often, lenses are shaped or curved in order to provide the equal path length condition needed to focus the energy. The closer the focal point, the thicker the lens must be. Since microwave lenses can be as much as several hundred wavelengths across [3], a thick lens made of standard dielectric material such as Rexolite could weigh as much as a 100 pounds or more. An alternative to shaping the lens is to constrain energy to travel along specific lengths of transmission line. These transmission lines could each be varied in length to accomplish the same result as shaping the lens. A lens that focuses energy in this way is known as a constrained lens [1]. Figure 2.1 shows the geometry of the constrained lens. Here, energy is received on one face of the lens by an array of antenna elements. Once the energy is received, the energy is then constrained to follow specific lengths of transmission lines and is then re-radiated by an array of antenna elements on the other face of the lens.

Constrained lenses have one distinct advantage over shaped or curved lenses in that they can be flat on both faces of the lens. Not only can the lens be made flat, but more importantly, the lens can be made thin. Since a thin lens would weigh

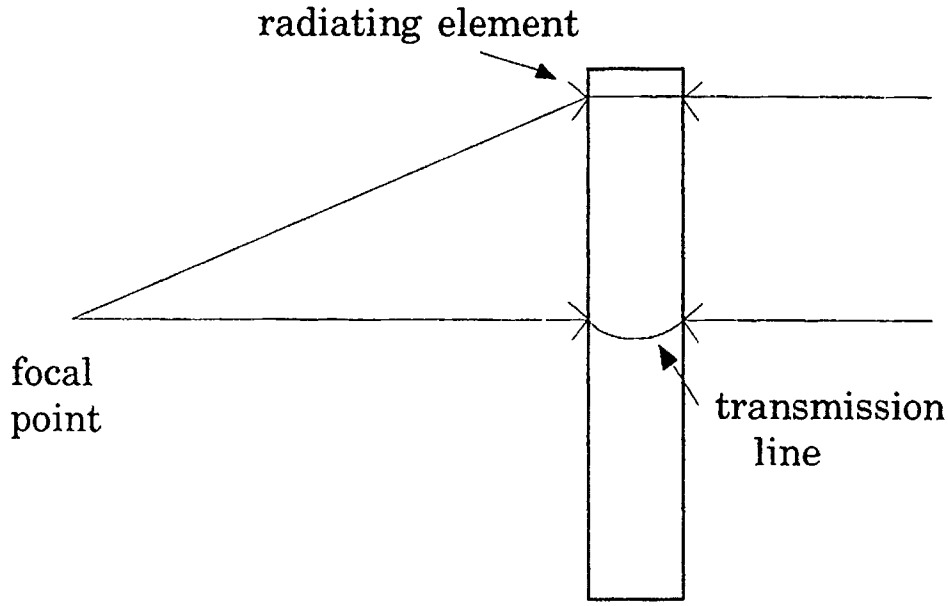

Figure 2.1. Geometry of the Constrained Lens

less than a thick lens of the same size and material, a constrained lens would be an optimum choice for a satellite or other space based system where weight is a primary concern.

Microwave lenses are generally used in applications where high gain or wide scanning capabilities are needed. A microwave lens can scan without actually moving the lens; all that is needed is to move the feed slightly off axis and the beam of the lens antenna scans proportionally. This feature is again important in space applications where it is better, for momentum reasons, to move smaller objects than larger ones.

Now that the reader has been introduced to the topic of microwave lenses and some of its applications, the topic of microwave lenses, and in particular constrained lenses, will be discussed.

2.3 Microwave Lenses

The idea of a microwave lens has been around at least since 1946 [4]. For the most part, many of the early design concepts are still valid and would still work well. The problem with the early designs was their weight; most were made out of metal waveguide or stacked metal plates. Even today with the use of dielectric materials such as Rexolite, the lens can be unacceptably heavy.

One method of reducing weight in a lens is using a technique known as zoning [3]. Zoning is based on the fact that electromagnetic waves are 2π periodic. By zoning a lens, you could remove some multiple number of wavelengths of material from the lens and still be able to focus energy as if the lens were not zoned. A zoned lens would have a stair step appearance across the face of the lens. One problem with zoning is that it is frequency dependent. By zoning a lens you have limited its usable bandwidth. Another problem with a zoned lens is shadowing, which is caused by non-uniform illumination of the lens. Shadowing occurs when the lens is scanned off-axis and results in higher sidelobes and filled-in pattern nulls. So, as mentioned earlier, the optimum choice in terms of weight is the thin flat lens or constrained lens.

The first documentation of a thin constrained lens appears in a paper by McGrath [5]. Here, an experimental model consisting of two planar arrays of microstrip-fed patch antennas is proposed. The patch antennas would then be connected by shorting pins as shown in Figure 2.2. It was concluded that a planar lens using the

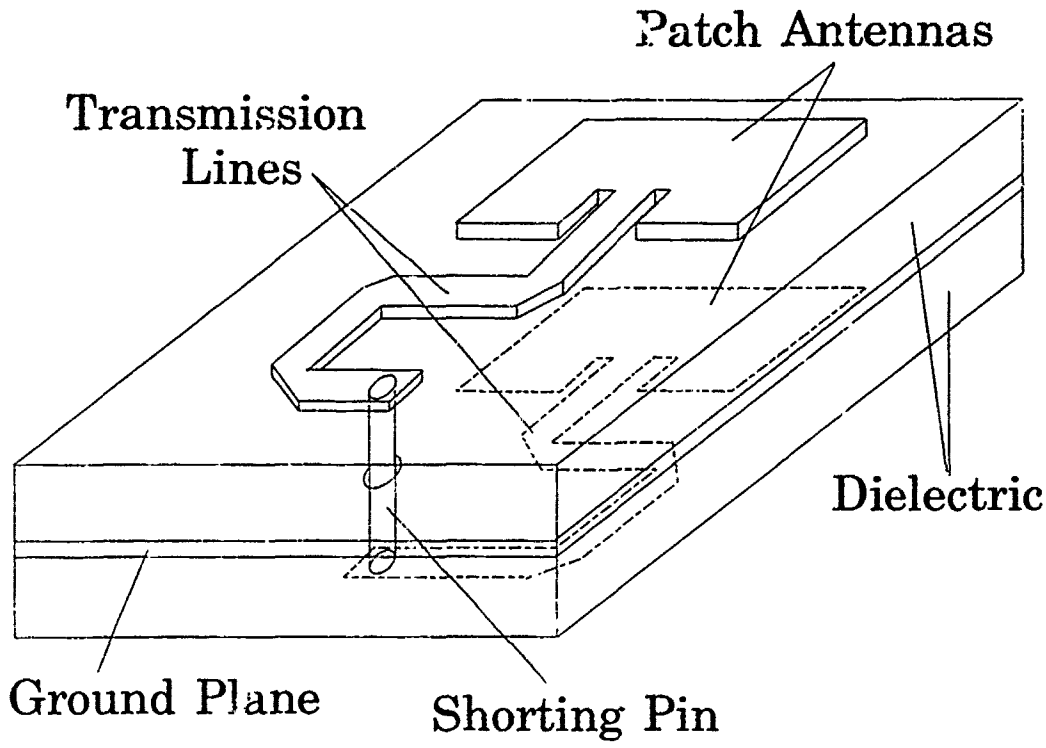

Figure 2.2. Microstrip Constrained Lens with Shorting Pins; Single Element

microstrip-fed patch antenna architecture would be both lightweight, and easy to fabricate using photolithographic techniques. The proposed model was not tested, but it was concluded that a two-degree-of-freedom lens in which positions of aperture- and feed-side elements are different allows substantially better off-axis performance than the single-degree-of-freedom design.

A later paper [6] by the same author describes the actual design and testing of the microstrip constrained lens proposed in [5]. In this microstrip lens design, small holes slightly larger than the diameter of the shorting pins were in the ground plane of the microstrip, as shown in Figure 2.2. The feedthrough holes were then drilled to allow for shorting pins to be installed. The shorting pins were then soldered to both the aperture-side microstrip lines and the feed-side microstrip lines. Since a lens antenna can have many hundreds of antenna elements, this shorting pin design can be labor intensive. The shorting pin architecture resulted in an overall lens efficiency of 29%, with the most significant loss mechanism attributed to the feedthrough pins. It was concluded that the lens could focus a quality beam (i.e. not much distortion) to ± 30 degrees in both azimuth and elevation planes.

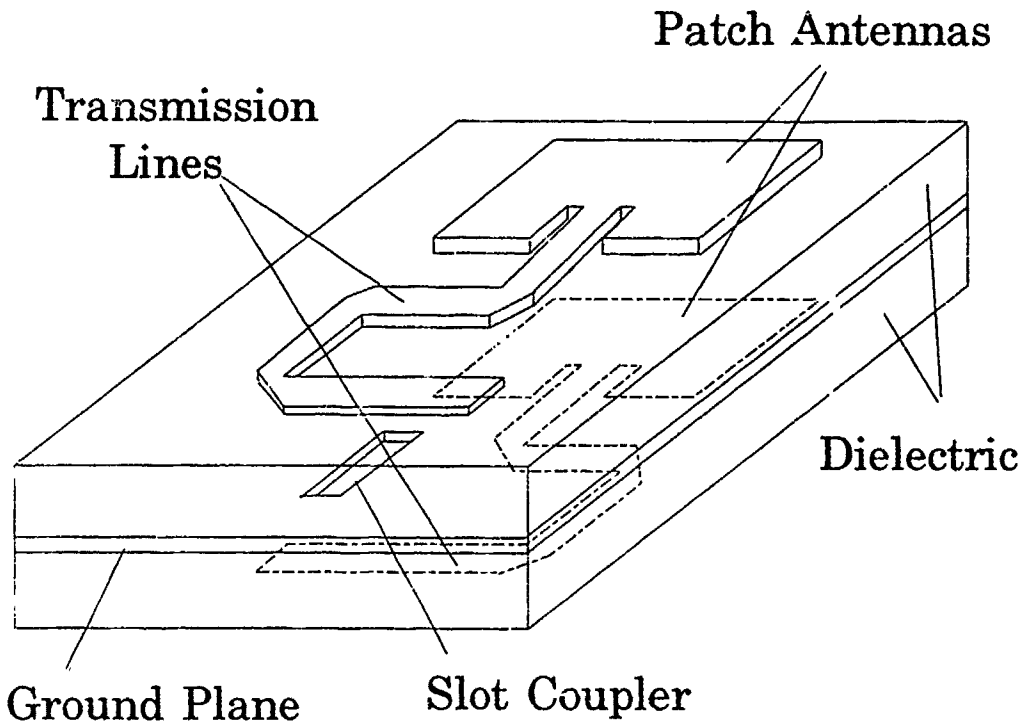

Figure 2.3. Microstrip Constrained Lens with Slot Coupling

The most recent paper [2] on the microstrip constrained lens again uses the microstrip patch antenna architecture but with a new feedthrough design as shown in Figure 2.3. In the new design, energy is electromagnetically coupled from one side of the lens to the other via a slot shaped aperture in the ground plane of the microstrip. This eliminates the labor-intensive drilling and soldering required in the shorting pin design. The slot coupler design was based on some preliminary slot coupler test results. However, a prototype slot coupler was not designed and tested prior to lens fabrication The result was a low efficiency lens. Two lessons that were learned from the slot coupler design were: 1) a new feedthrough design and a low-loss dielectric substrate would increase lens efficiency substantially and 2) the close proximity of microstrip transmission lines to the radiating edge of the patch needs to be avoided in order to prevent interference between microstrip lines and patch radiators.

2.4 Conclusion

A thin flat lens design would be an optimum choice in terms of weight. The slot coupled microstrip constrained lens has the potential to satisfy a thin lens design criterion. The slot coupled lens would also be lightweight and easy to fabricate using photolithographic techniques. The use of a low-loss dielectric substrate would increase lens efficiency substantially. It is determined that the microstrip constrained lens can focus quality beams to moderately wide scan angles in both the azimuth and elevation planes. The close proximity of microstrip transmission lines to the radiating edge of the patch needs to be avoided in order to prevent interference between microstrip lines and patch radiators.

III. Slot Coupler

3.1 Introduction

This chapter covers the design, fabrication and testing of the prototype slot coupler used in the lens design. Since finding a slot coupler with minimal insertion loss was critical to designing a lens with high overall efficiency, the slot coupler was designed and tested separate from the lens. In this way, a number of different slot coupler designs could be tried at minimal cost in time and material. The slot coupler design that resulted in the smallest insertion loss was then used in the lens design. This two step procedure reduced risk of failure in designing a high efficiency lens. Also, by testing the slot couplers separately, loss mechanisms in the slot coupler could be measured and evaluated independently from the lens.

An exact model for the slot coupler does not exist in the literature, therefore, an approximate model is used in the slot coupler design. It should be kept in mind throughout this chapter that the main goal of using the prototype slot coupler was to find a slot coupler design that would result in minimum insertion loss. It is not a goal of this thesis to derive a new model for the slot coupler in order to accurately predict test results.

This chapter is broken up into four sections. First, an approximate model for the microstrip-slot-microstrip transition is introduced along with the equations used in the slot coupler design. Each design parameter in the model will be discussed, including the topics of line losses and end effects. Second, fabrication of the slot coupler is covered, including material selection and a brief description of the fabrication process. Third, the testing and results of the prototype slot coupler designs are discussed and the results are compared to theory. Finally, the chapter ends with some concluding remarks.

3.2 Prototype Design

3.2.1 Model A diagram of the slot coupler is shown in Figure 3.1. The slot coupler consists of two low-loss dielectric substrates sharing a common ground plane. Microstrip transmission lines are etched on both the top and bottom faces of the substrates and a slot is etched in the ground plane. The coupler works by guiding

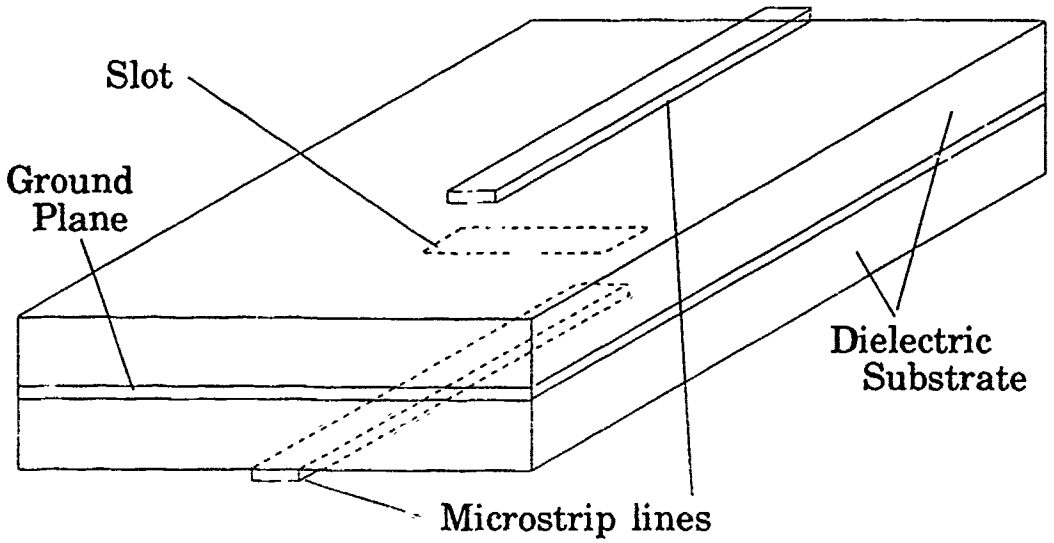

Figure 3.1. Slot Coupler

microwave energy down a specific length of microstrip transmission line, then coupling the energy to a second microstrip transmission line via a slot in the ground plane. Ideally, all the energy that is received on the first microstrip line will be coupled onto the second line. In reality however, a small portion of the energy will be reflected back onto the first line because of an impedance mismatch that occurs at the slot. The less energy that is reflected back onto the first line, the more efficient the slot design. It is the design of this slot coupler that will be covered in this section. More discussion on efficiency (or losses) will follow.

The slot coupler is essentially a microstrip-slot-microstrip transition. As already mentioned, such a transition does not appear in the literature. If, however, this one transition is broken up into two transitions, one would see first a microstrip-slot transition followed by a second slot-microstrip transition. This helps the situation, since the microstrip-slot transition does appear in the literature. Also, since the microstrip slot and slot-microstrip transition are identical, optimization of one transition will result in the optimization of the second transition. In the following development, only the microstrip-slot transition is treated. Two of the slot param-

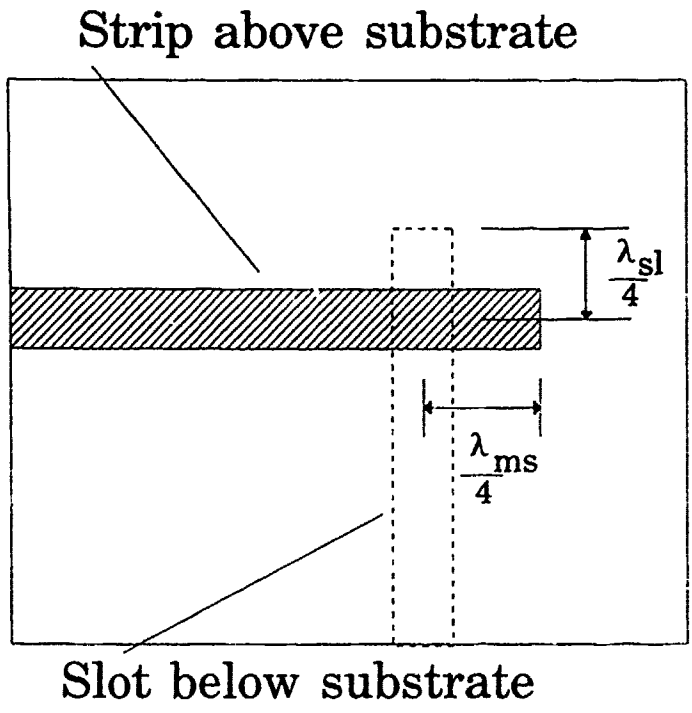

Figure 3.2. Microstrip-Slot Transition

eters, however, will be changed in order to account for loading of the slotline by the second substrate. It is the microstrip-slot transition that forms the basis for modeling the microstrip-slot-microstrip transition.

A diagram of the microstrip-slot transition is shown in Figure 3.2. The transition consists of dielectric substrate with a microstrip line etched on one side of the substrate and a slot line etched on the other side of the substrate. The microstrip and slot lines cross at right angles to, and extend about a quarter guide wavelength beyond, each other.

An equivalent circuit for the microstrip-slot transition is given by Knorr [7]. The equivalent circuit is shown in Figure 3.3 where

Z_{sl} = slot impedance,

θ_{sl} = electrical length of slot stub,

X_{sl} = reactance of shorted stub.

Z_{ms} = microstrip impedance,

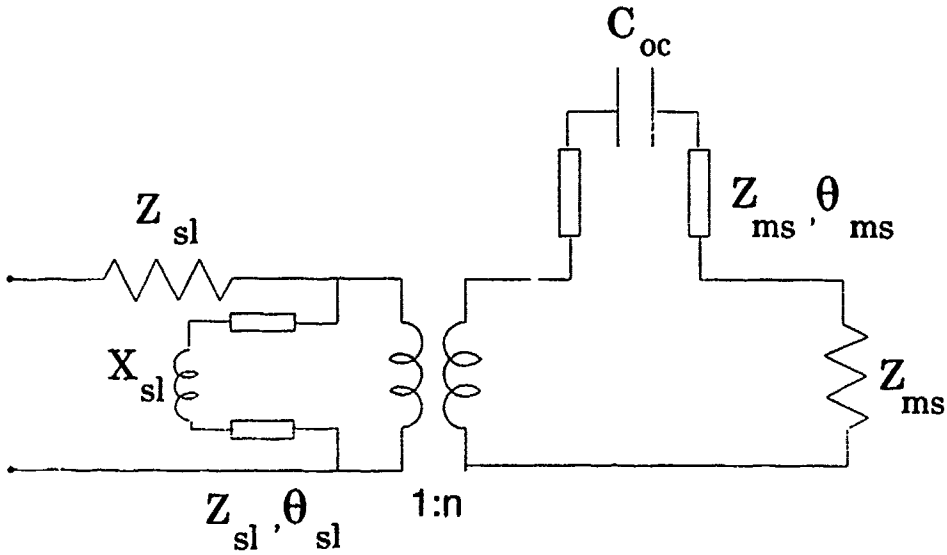

Figure 3.3. Equivalent Circuit for the Microstrip-Slot Transition

θ_{ms} = electrical length of microstrip stub,

C_{oc} = equivalent capacitance of open microstrip.

The transformer ratio, n, is determined from knowledge of slotline field components. In the approximate analysis reported by Knorr [7], n is defined as

$$n = \cos\left[2\pi\frac{h}{\lambda_0}u\right] - \cot q_0 \sin\left[2\pi\frac{h}{\lambda_0}u\right] \tag{3.1}$$

with

$$q_0 = \frac{2\pi u}{\lambda_0}h + \tan^{-1}[u/v] \tag{3.2}$$

$$u = \left[\epsilon_r - \left(\frac{\lambda_0}{\lambda_s}\right)^2\right]^{1/2} \tag{3.3}$$

$$v = \left[\left(\frac{\lambda_0}{\lambda_s}\right)^2 - 1\right]^{1/2} \tag{3.4}$$

where λ_s is the slot wavelength, h is the thickness and ϵ_r is the relative dielectric constant of the substrate.

From inspection of the circuit in Figure 3.3, it is seen that one can obtain a perfect match at a given frequency by making

$$Z_{sl} = \frac{Z_{ms}}{n^2} \tag{3.5}$$

$$B_{sl}^{in} = 0 \tag{3.6}$$

$$X_{sl}^{in} = 0 \tag{3.7}$$

where B_{sl}^{in} is the susceptance looking into the shorted slot stub and X_{sl}^{in} is the reactance looking into the open-circuited microstrip stub.

With the basic model for the microstrip-slot transition now defined, the following subsections will be devoted to determining the parameters $Z_{ms}, Z_{sl}, \theta_{sl}, \theta_{ms}, \lambda_s$.

3.2.2 Microstrip Line Microstrip transmission lines have been well documented and tested. There are also many computer-aided design packages available

for determining the correct microstrip line width for a given set of substrate parameters and characteristic impedance. One program that the author has been successful with, which takes into account such things as conductor thickness and effective dielectric constant, appears in a Rome Laboratory Technical Report [8]. The program is written in FORTRAN, and is based on microstrip design equations found in [9]. The equations are repeated here for completeness.

$$Z_{ms} = \frac{\eta}{2\pi\sqrt{\epsilon_{re}}} \ln\left[\frac{8h}{W_e} + 0.25\frac{W_e}{h}\right] \qquad (W/h \leq 1) \qquad (3.8)$$

$$Z_{ms} = \frac{\eta}{\sqrt{\epsilon_{re}}}\left[\frac{W_e}{h} + 1.393 + 0.667\ln\left(\frac{W_e}{h} + 1.444\right)\right]^{-1} \qquad (W/h \geq 1) \qquad (3.9)$$

where

$$\frac{W_e}{h} = \frac{W}{h} + \frac{1.25}{\pi}\frac{t}{h}\left(1 + \ln\frac{4\pi W}{t}\right) \qquad (W/h \leq 1/2\pi) \qquad (3.10)$$

$$\frac{W_e}{h} = \frac{W}{h} + \frac{1.25}{\pi}\frac{t}{h}\left(1 + \ln\frac{2h}{t}\right) \qquad (W/h \geq 1/2\pi) \qquad (3.11)$$

$$\epsilon_{re} = \frac{\epsilon_r + 1}{2} + \frac{\epsilon_r - 1}{2}F(W/h) - C \qquad (3.12)$$

in which

$$C = \frac{\epsilon_r - 1}{4.6}\frac{t/h}{\sqrt{W/h}} \qquad (3.13)$$

$$F(W/h) = (1 + 12h/W)^{-1/2} + 0.04(1 - W/h)^2 \qquad (W/h \leq 1) \qquad (3.14)$$

$$F(W/h) = (1 + 12h/W)^{-1/2} \qquad (W/h \geq 1) \qquad (3.15)$$

In the above equations, t is the thickness of the conductor, W is the width of the microstrip line and $\eta = 120\pi$ ohms. The effect of conductor thickness is insignificant for $t/h \leq 0.005, 2 \leq \epsilon_r \leq 10$ and $W/h \geq 0.1$. However, the effect of conductor thickness is significant on conductor loss in the microstrip line.

Calculation of the microstrip stub length θ_{ms} is based on the effective dielectric constant ϵ_{re} computed above.

$$\theta_{ms} = \frac{\lambda_0}{\sqrt{\epsilon_{re}}} \tag{3.16}$$

3.2.3 Microstrip Losses One thing that will have to be accounted for when calculating the overall loss in the lens design is the loss due to attenuation in the microstrip line. Microstrip line has two primary types of loss associated with it, conductor loss α_c and dielectric loss α_d. The total loss α_T is equal to the sum of the two: $\alpha_T = \alpha_c + \alpha_d$. The dielectric loss is generally small when compared with conductor loss on dielectric substrates. Closed form equations for calculating α_c and α_d expressed in dB per unit length are given by [9]:

$$\alpha_c = \begin{cases} 1.38A\frac{R_s}{hZ_{ms}}\frac{32-(W_e/h)^2}{32+(W_e/h)^2} & (W/h \leq 1) \\ 6.1\times 10^{-5}A\frac{R_s Z_{om}\epsilon_{re}}{h}[W_e/h + \frac{0.667W_e/h}{W_e/h+1.444}] & (W/h \geq 1) \end{cases} \tag{3.17}$$

and

$$\alpha_d = \begin{cases} 4.34\eta\sigma\frac{\epsilon_{re}-1}{\sqrt{\epsilon_{re}}(\epsilon_r-1)} & (W/h \leq 1) \\ 27.3\frac{\epsilon_r}{\epsilon_r-1}\frac{\epsilon_{re}-1}{\sqrt{\epsilon_{re}}}\frac{\tan\delta}{\lambda_0} & (W/h \geq 1) \end{cases} \tag{3.18}$$

where

$$A = 1 + \frac{h}{W_e}\left[1 + \frac{1.25}{\pi}\ln\frac{2B}{t}\right] \tag{3.19}$$

$$R_s = \sqrt{\pi f \mu_o/\rho_c} \tag{3.20}$$

and

$$B = \begin{cases} h & (W/h \leq \frac{1}{2\pi}) \\ 2\pi W & (W/h \geq \frac{1}{2\pi}) \end{cases} \tag{3.21}$$

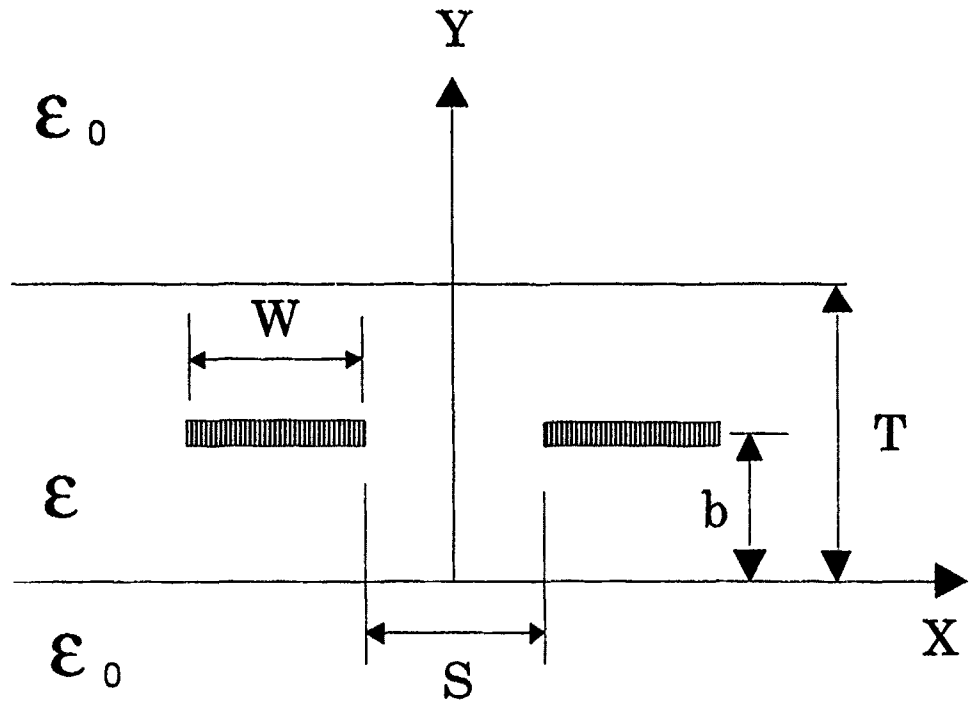

Figure 3.4. Slotline Geometry

In the above equations, ρ_c is the resistivity of the strip conductor, μ_0 is the permitivity of free space, $\sigma = \omega\epsilon_0\epsilon_r \tan\delta$ is the conductivity of the dielectric substrate and $\tan\delta$ the loss tangent. The remaining parameters are as before.

3.2.4 Slotline Most papers on the topic of slotline only treat slotline used in the conventional sense, that is, with the slotline etched on top of the substrate. However, in the microstrip-slot-microstrip transition, the slotline is sandwiched between two substrates. The geometry for the sandwiched slotline is shown in Figure 3.4. Here, two conducting strips of width W are separated by slot width S, and are embedded between two dielectric substrates of thickness T.

A recent paper by Lee [10] that treats sandwiched slotline and is general in nature was the foundation for the calculation of the slot parameters Z_{sl} and λ_s. The paper first solves the Green's function for a pair of filament sources embedded in a dielectric substrate. The Green's function was then used to construct the total potential arising from two conducting strips embedded in a substrate. Then the surface charge density on the conducting strips is found by using a moment method

and imposing the source condition (equal potential) on the conductors. Using Lee's equations, the total charge Q is then

$$Q = \sum_{j=1}^{N} q_j = \sum_{j=1}^{N}\sum_{i=1}^{N} C_{ij} V \tag{3.22}$$

where

$$[C_{ij}] = [P_{ij}]^{-1} \tag{3.23}$$

$$\begin{aligned} P_{ij} \;=\; & \frac{1}{2\pi\epsilon} \ln \frac{x_j + x_i}{|x_j - x_i|} + \frac{\epsilon_-}{\pi\epsilon} \int_0^\infty \frac{\sin k_x x_i \sin k_x x_j}{k_x(\epsilon_+^2 - \epsilon_-^2 e^{-2k_x T})} \times \\ & [\epsilon_+ e^{-2k_x(T-y_0)} + 2\epsilon_- e^{-2k_x T} + \epsilon_+ e^{-2k_x y_0}] dk_x \end{aligned} \tag{3.24}$$

With Q determined, the unit capacitance of the slotline is computed by

$$C' = \frac{Q}{2V} = \frac{1}{2}\sum_{j=1}^{N}\sum_{i=1}^{N} C_{ij} \tag{3.25}$$

The factor 2 accounts for the fact that the two strips are charged to plus and minus V volts with a difference of $2V$ volts. From this capacitance the characteristic impedance, wavelength and effective dielectric constant can be computed by

$$Z_{sl} = (C_0/C')^{1/2} Z_0 \tag{3.26}$$

$$\lambda_{sl} = (C_0/C')^{1/2} \lambda_0 \tag{3.27}$$

$$\epsilon_{eff} = C'/C_0 \tag{3.28}$$

where Z_0 and C_0 are the characteristic impedance and unit capacitance of the slotline when there is no dielectric loading of the substrate, and $Z_0 = (c_0 C_0)^{-1}$, with c_0 being the speed of light in free space. In the moment method above, delta functions are

used as the basis and test functions. For prototype calculations, the strip was divided into 60 segments, and the integral was truncated at a finite point. It was found that a wavenumber of 8000 for k_x is more than adequate to yeild an accurate solution. When $i = j$ in the above equations, it is necessary to offset x_i slightly to avoid the singularity in the logarithmic term. The author used an offset of $1\mu m$ for slot calculations.

3.2.5 End Effects Because an open-ended microstrip line has fringing fields that extend beyond the conductor itself, a length extension is required to account for the apparent increase in electrical length due to an open-ended stub. Hammerstad gives a good approximation for the apparent length extension as [11]:

$$\Delta l = 0.412h \frac{(\epsilon_{re} + 0.3)}{(\epsilon_{re} - 0.258)} \frac{(W/h + 0.264)}{(W/h + 0.8)} \tag{3.29}$$

With all the microstrip parameters Z_{ms}, θ_{ms} and length extension Δl determined, the next step is to look at losses in the microstrip line.

As in the case of an open-ended microstrip line, a shorted slotline also requires a length correction due to currents that flow around the end of the slot. The result is stored magnetic energy just beyond the termination which give rise to an inductive reactance. The end effect is significant and the electrical length θ_{sl} of the slot can be as much as $0.1\lambda_s$ greater than the physical length of the slot [12]. Since a slot coupler has two shorted ends this effect is doubled. While there are no analytical results [9] for evaluating the shorted discontinuity, there is a limited amount of experimental results available [12]. Parametric curves of [12] are used to determine the slot length extension Δl_{sl}. Once Δl_{sl} is determined, the following equation is used to determine the physical slot length SL.

$$SL = \frac{\lambda_s}{2} - 2\Delta l_{sl} \tag{3.30}$$

3.3 Fabrication

3.3.1 Fabrication Process Slot coupler fabrication consists of a three-step process. First, a computer pen-plot is generated of the circuit layout. A liquid ink pen plotter with a paper handling capability that is at least twice the size of the circuit is preferred. Often, a pen-plot is generated that is two to four times

larger than the actual circuit. The pen-plot will later be photographically reduced to desired size. This method helps reduce errors in the plot due to inaccuracies of the plotter itself. Second, the pen-plot is taken to the photolab, where a photographic negative is taken of the plot. The negative produced (also known as the mask) should be reduced to the desired size. Finally, the mask and a piece of copper-cladded substrate are sent out to a foundry where portions of the copper are chemically removed from the substrate. Etching was accomplished at Wentworth Industries, Newton MA, through a service contract with Rome Laboratory.

The slot coupler is a multiple layer design with a single ground plane (which contains the slots) sandwiched between two substrates. Generally, substrates are purchased with copper cladding on both sides of the substrate. In order to make alignment of the layers simpler, one substrate has its copper cladding totally removed from one of its faces during fabrication. The layers are then epoxied together using a two part conducting epoxy that cures at room temperature. The brand of epoxy used for both the prototype slot couplers and the lens was a silver-based conducting-epoxy made by Epoxy Technology Inc., Billerica MA, part number H20E. The epoxy was spread thinly using a razor blade and was allowed to cure for ten days at room temperature.

3.3.2 Prototype Slot Coupler Layout The substrate used for both slot coupler designs and lens fabrication was 0.05 inch thick RT Duroid with 1/2 ounce copper cladding. The substrate has a relative dielectric constant $\epsilon_r = 6.0$ and a loss tangent $tan\delta = 0.0027$. The substrate was available in 20 by 20 inch sheets. This substrate was selected for both its low-loss properties, its relatively high dielectric constant and its availability. Choosing a substrate with a higher dielectric constant means both smaller microstrip line widths and patch antenna dimensions as compared to a more common $\epsilon_r = 2.5$ material. These smaller dimensions will be important later when laying out the lens, as patch antennas, slot couplers and microstrip lines all compete for the same area on the surface of the substrate. For the reason of reduced line width, an 80Ω microstrip line will be used to feed patch antennas in the lens rather than the standard 50Ω line. For example, an 80Ω line has a width of 0.0235 inches on the mentioned substrate. This is about 1/3 the microstrip line width used in previous lens designs [2], [6].

Eight prototype slot couplers were designed and fabricated. Each slot coupler consisted of two, 2 by 2.5 inch substrates. Each substrate had a 80Ω microstrip

line etched on one surface of them, and as already mentioned, one of the substrates had its ground plane totally removed. The other substrate had a slot etched into its ground plane. Flange mount jack-tab connectors were then soldered to one end of the microstrip line in order to provide the interface between microstrip line and test equipment. Since an SMA jack-tab connector has an impedance of 50Ω, a 63Ω quarterwave transformer was then used to match the jack-tab connector to the 80Ω microstrip line. The jack-tab connectors have a tab width of 0.02 inches and can be purchased through Omni Spectra, P/N 2052-5636-00. Microstrip line dimensions were exactly the same for all eight slot couplers, the only difference between the eight candidates were the dimensions of the slots which will be listed in Section 3.4.2.

3.4 Testing

3.4.1 Calibration and Set-up It was not possible to calibrate the HP 8510 Automatic Network Analyzer up to the SMA jack-tab connectors. Since only a 7mm calibration kit was available, calibration was only possible to the ends of the 7mm test cables. Four adapters (two on each port) were then required to mate the female SMA jack-tab connectors on the unit under test to the 7mm test cables. Because of this, the actual insertion loss will be less than what was measured. The test set up is shown in Figure 3.5.

3.4.2 Measurements The slot couplers were then tested for insertion loss in the 7.5 to 8.5 GHz frequency band. A time-domain measurement was also made to see, on a relative scale, where major reflections were coming from. The slot coupler with the lowest insertion loss was then chosen for the lens design. All insertion loss measurements were made on an HP 8510 Automatic Network Analyzer. Figure 3.6 shows the insertion loss measurement for the slot coupler that was chosen for the lens design. The slot has a length of 0.346 inches and a width of 0.03 inches. It can be seen in Figure 3.6 that the insertion loss varies between 1.2 and 1.9 dB over the 7.5 to 8.5 GHz band, with about 1.6 dB insertion loss at the 8.0 GHz design frequency. Keep in mind that this measurement includes both losses due to attenuation in the microstrip line, and the extra hardware used in the calibration. A theoretical plot generated from the model developed in Section 3.2.1 is shown in Figure 3.7. The model predicts an insertion loss of about 0.93 dB at the 8.0 GHz design frequency. If we take into account that more insertion loss will be added to this value because

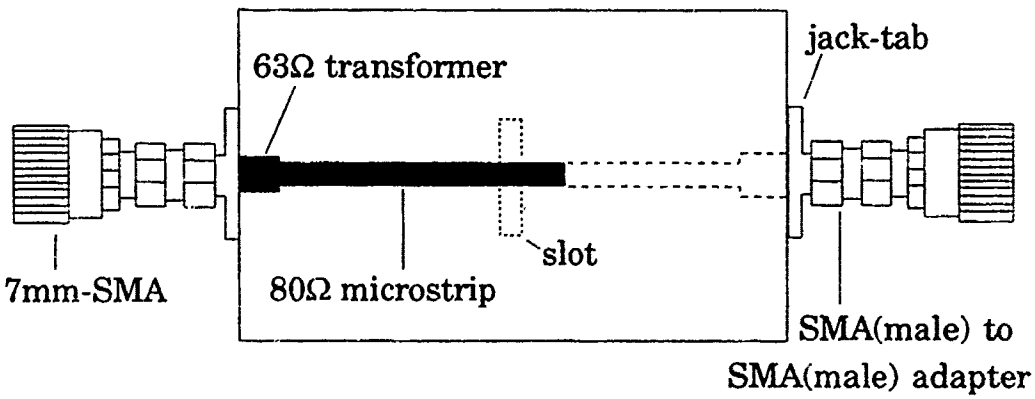

Figure 3.5. Setup for Testing the Prototype Slot Couplers

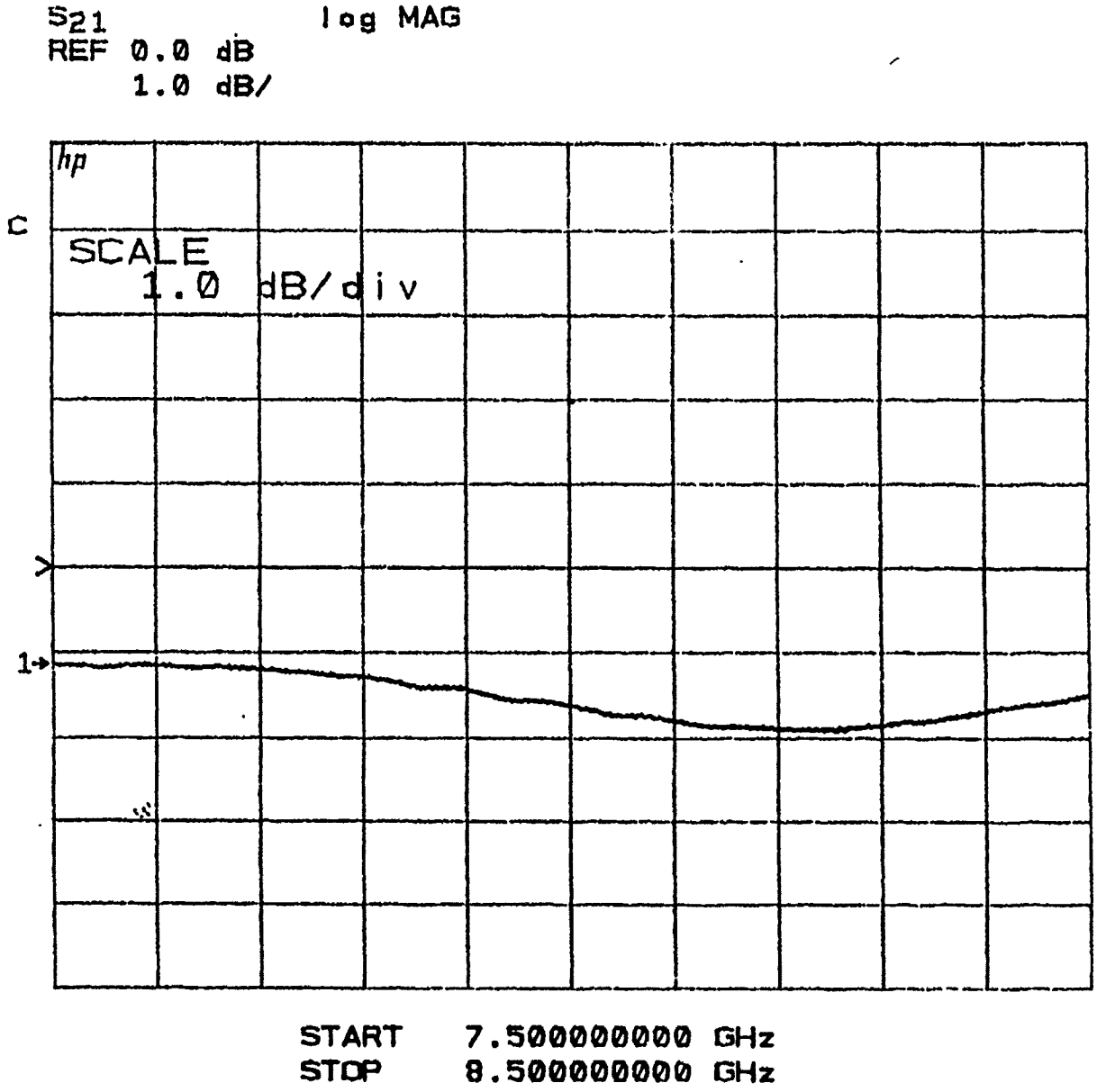

Figure 3.6. Insertion Loss, SL=0.346 Inches, SW=0.03 Inches

Candidate #	*Slot Length* SL(inches)	*Slot Width* SW(inches)	*Theory* (dB)	*Measured* (dB)
1	0.346	0.03	0.9	1.6
2	0.390	0.03	0.7	2.3
3	0.433	0.03	1.2	3.1
4	0.425	0.02	1.6	3.4
5	0.340	0.02	1.8	1.6
6	0.412	0.02	2.5	2.8
7	0.371	0.01	2.5	2.2
8	0.330	0.01	3.0	1.8

Table 3.1. Measured Insertion Loss vs Theory on Candidate Slot Couplers at 8.0 GHz

of line loss and extra hardware, the model seems to reasonably predict measured results for candidate #1 slot. In Table 3.1 we see that the model does fall apart somewhat on some of the other candidate slots. For example, the difference between the theoretical and measured insertion loss for candidate slot #3 is 1.9 dB.

One thing that did stand out about the measured data was that the slots with shorter physical lengths (and hence shorter electrical lengths) had lower measured insertion losses than the slots with longer physical lengths. The slots with the lowest measured insertion loss (candidates #1, #5, and #8) all had electrical lengths (including fringing) in the $0.400\lambda_s - 0.440\lambda_s$ range, while the slots with the highest insertion losses (such as candidates #3, #4 and #6) had electrical lengths in the $0.494\lambda_s - 0.528\lambda_s$ range. Hence, future slot coupler designs should have slots whose electrical lengths fall in the $0.400\lambda_s - 0.440\lambda_s$ range.

Note the theoretical insertion loss column of Table 3.1 suggests a slot of width 0.03 inches should have a lower insertion loss than a slot of width 0.01 inches. Also, the insertion loss should not be strongly dependent on slot length. A slot of width 0.03 inches was in fact chosen for the lens design, however, measured data supports a stronger dependence on slot length than slot width.

The remaining seven measurements are all similar to Figure 3.6 varying only in relative amplitude. The reader is referred to Appendix A for the remaining seven insertion loss measurements. One characteristic common to all seven plots was the slow oscillation of insertion loss between its maximum and minimum value. In all

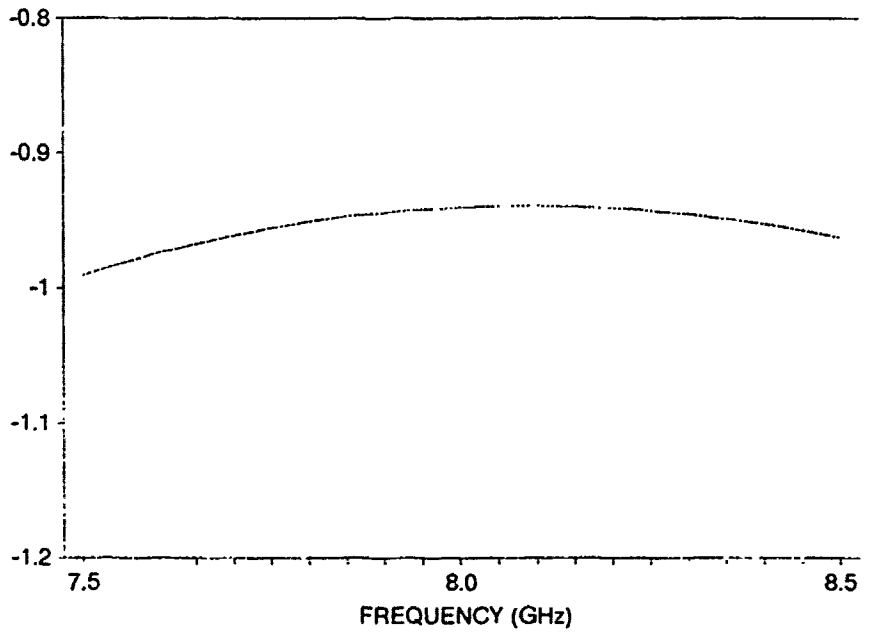

Figure 3.7. Theoretical Insertion Loss for SL=0.346 Inches, SW=0.03 Inches

seven plots, minimum insertion loss occurred around 7.5 GHz and the maximum insertion loss occurred around 8.2 GHz. Since the only difference between the eight measurements were the dimensions of the slot, moving the minimum insertion loss level from the 7.5 GHz to the 8 GHz design frequency might be possible by changing the microstrip stub length, since slot dimensions seemed to have no effect on shifting the minimum insertion loss position. It is also possible that the slow oscillation is an interference pattern caused by three dominant reflection points. These three reflection points are shown in the time domain measurement.

A time-domain reflection measurement was performed on the slot with dimensions $SL = 0.346$ inches and $SW = 0.03$ inches; the results are shown in Figure 3.8. Since reflection measurements require only one port, the second port was terminated with a 50Ω load.

Significant points in Figure 3.8 are as follows. Point 1 is where a transition is made from the 50Ω jack-tab to microstrip line. Point 2 is where the microstrip-slot-microstrip transition is made. Point 3 is where the microstrip to jack-tab connection is made and terminated with a 50Ω load. Points 1 and 3 were precisely identified by loosening the connector slightly and observing the rise in reflection at that point. By comparing the relative amplitudes of the three points we see that the microstrip-slot-microstrip transition is only slightly worse than the two microstrip-jack tab transitions. It has been the authors experience that a well soldered jack-tab typically has an insertion loss in the neighborhood of 0.3 dB.

3.5 Conclusion

A prototype slot coupler was successfully designed, fabricated, and tested. Total insertion loss through the slot coupler, including attenuation in the microstrip line and some extra calibration hardware, was 1.6 dB at the 8.0 GHz design frequency. It was determined that more optimization may be possible by changing the microstrip stub length. Also, a slot with an electrical length (including fringing) in the $0.400\lambda_s - 0.410\lambda_s$ range seems to be optimum in terms of insertion loss for the microstrip-slot microstrip transition.

This was the first time that a model for the microstrip-slot-microstrip transition has been documented. This model was useful in predicting measured insertion loss results. The model seemed to work reasonably well for some slots that were tested

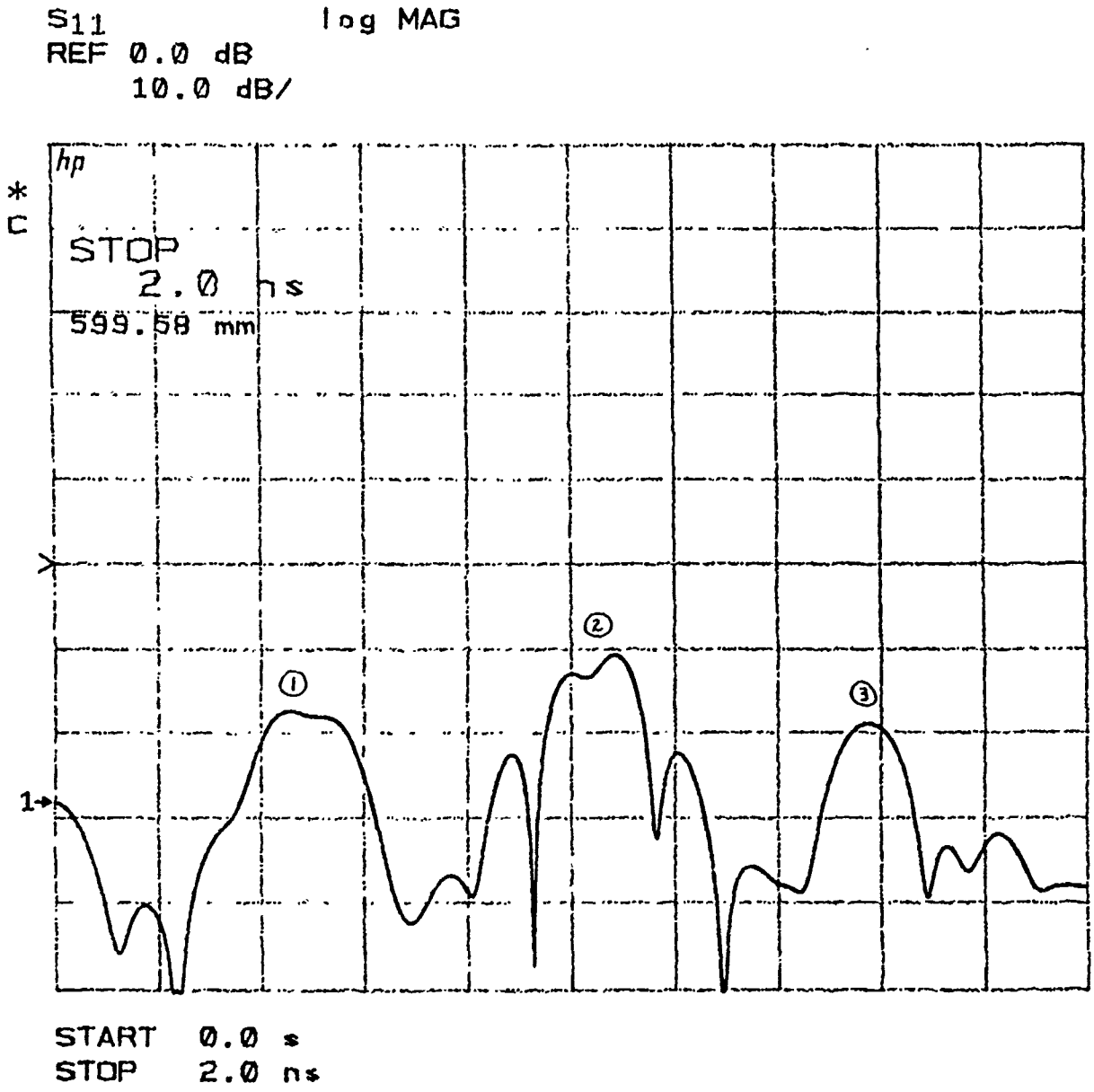

Figure 3.8. Time Domain Reflection Measurement, SL=0.346 Inches, SW=0.03 Inches

but was off by as much as 1.9 dB on one other slot that was tested. For this reason, it is suggested that the model be used only in baseline designs until a more accurate model is found.

IV. Lens

4.1 Introduction

This chapter covers the design and testing of the planar microwave lens. The chapter is divided into four sections. The first section discusses the design equations used in determining the patch antenna dimensions and transmission line lengths. The second section discusses the fabrication of the lens. This discussion includes the strategy for laying out the patch antennas and the transmission lines, as well as a strategy for selecting a polarization for aperture- and feed-side antenna elements. The third section covers the testing of the lens design. Here, both on-axis radiation patterns of the lens will be presented, along with radiation patterns taken with the feed moved to various scan angles. The third section ends with a determination of overall lens efficiency. Finally, the chapter ends with some concluding remarks.

4.2 Lens Design

4.2.1 Patch Antennas Patch antennas were used as the radiating elements of the microwave lens because they are light in weight, highly efficient and easy to fabricate. They have symmetric $\cos\theta$ radiation patterns and are easily arrayed. One disadvantage of using the patch antenna is its narrow bandwidth, which is typically on the order of a few percent. This will not be a problem for this thesis, but could be a limiting factor in some lens applications requiring a wider bandwidth.

Two things were decided upon early in the lens design. First was the resonant frequency of the patch. For this thesis, an 8.0 GHz patch was used so that lens performance could be compared to the previous lens designs of [2] and [6]. Second was the input impedance to the patch. For reasons that will be explained later, an 80Ω feed line was used. The following paragraphs describe the design equations used in determining the patch dimensions.

Feeding a patch antenna is not as easy as simply attaching a transmission line to the edge of the patch. This is because the input impedance of a rectangular patch antenna can be as high as 300Ω when fed from the edge. Thus, in order to match the edge impedance of the patch to a transmission line, a quarterwave transformer is typically used. An alternative to using a transformer is to move the feed point

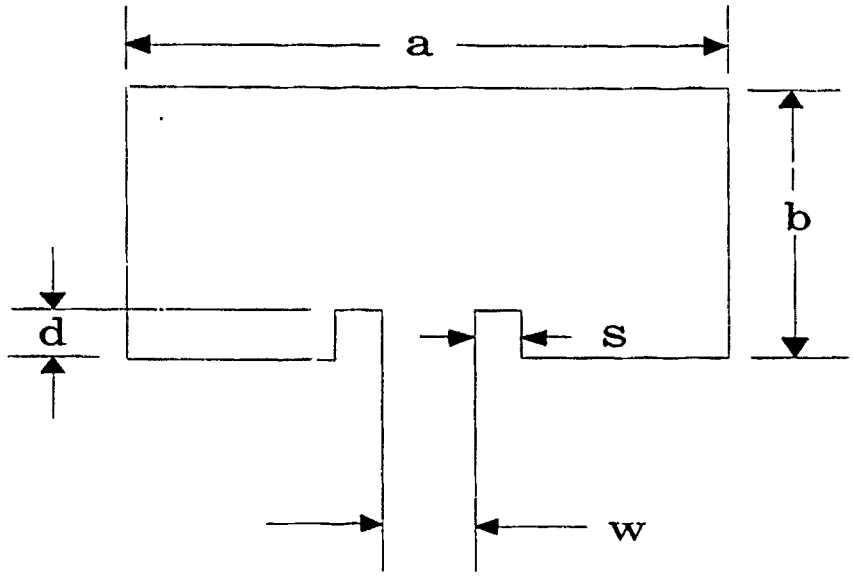

Figure 4.1. Inset Feed Patch Antenna

on a pat antenna in toward the center of the patch, where a much lower input impedance can be obtained. This is the idea behind the inset feed patch antenna. An inset feed rectangular patch antenna is shown in Figure 4.1. The rectangular patch has length b and width a. Note that the feed point has been moved inward from the patch edge by etching two slots, of length d and width s, parallel to the microstrip feed line. With the use of the inset feed patch antenna we can connect the microstrip line of width w directly to the rectangular patch without the use of a quarterwave transformer.

A simple but accurate transmission line model [13] is then used to determine the input impedance of an inset feed patch antenna. In the transmission line model, the radiating edges of the patch are modeled as two slots, radiating into free space, separated by a section of microstrip line. By determining the impedance of the slots and then referring the slot impedances back to the feed point, we can determine the input impedance of the patch antenna. The transmission line model is shown in Figure 4.2. Since the following equations involve a parallel network, it is simpler to work with slot admittances rather than slot impedances. The transmission line model has front slot admittance Y_{s1} and rear slot admittance Y_{s2}. The slot admittances Y_{s1} and Y_{s2} are located at distances d and $(b-d)$ respectively from the feed point. By adding the two referred admittances Y_1 and Y_2, the following expression for input

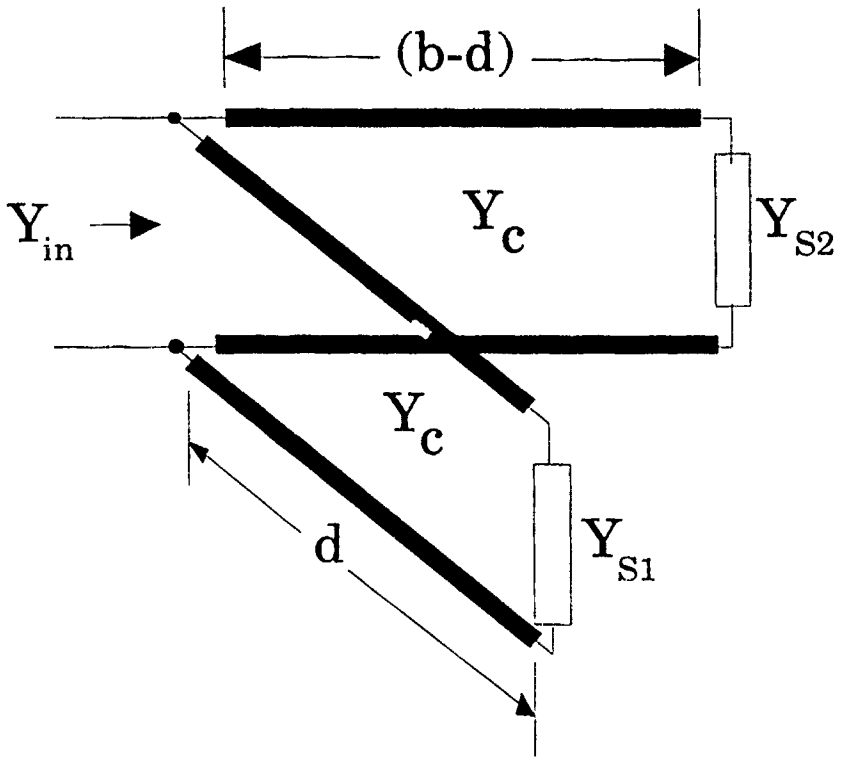

Figure 4.2. Transmission Line Model for the Patch Antenna

admittance Y_{in} is obtained:

$$Y_{in} = Y_1 + Y_2 \tag{4.1}$$

where

$$Y_i = \frac{e^{jx_i} - \Gamma_i e^{-jx_i}}{e^{jx_i} + \Gamma_i e^{-jx_i}} Y_c \qquad i = 1,2 \tag{4.2}$$

$$\Gamma_i = \frac{Y_c - Y_{si}}{Y_c + Y_{si}} \qquad i = 1,2 \tag{4.3}$$

with

$$Y_c = \frac{\sqrt{\epsilon_{re}}}{\eta_0} \left[\frac{a_e}{h} + 1.393 + 0.667 \ln \left(\frac{a_e}{h} + 1.444 \right) \right]^{-1} \tag{4.4}$$

$$Y_{s1} = \frac{\pi(a-2w)}{\lambda_0 \eta_0} \left[1 - \frac{(kh)^2}{24} \right] + j \frac{a-2w}{\lambda_0 \eta_0} \left[3.135 - 2 \ln (kh) \right] \qquad \left(\frac{h}{\lambda_0} \leq 0.1 \right) \tag{4.5}$$

$$Y_{s2} = \frac{\pi a}{\lambda_0 \eta_0} \left[1 - \frac{(kh)^2}{24} \right] + j \frac{a}{\lambda_0 \eta_0} \left[3.135 - 2 \ln (kh) \right] \qquad \left(\frac{h}{\lambda_0} \leq 0.1 \right) \tag{4.6}$$

$$a_e = a + \frac{1.25t}{\pi} \left[1 + \ln \left(\frac{2h}{t} \right) \right] \qquad \left(a \geq \frac{h}{2\pi} \right) \tag{4.7}$$

$$x_1 = kd\sqrt{\epsilon_{re}} + k\Delta l \tag{4.8}$$

$$x_2 = k(b-d)\sqrt{\epsilon_{re}} + k\Delta l \tag{4.9}$$

The parameters Δl, η_0, h, t, and ϵ_{re} were defined in Chapter 3, and $k = 2\pi/\lambda_0$. To determine the correct patch dimensions for a given resonant frequency, the following procedure is used [13]:

a. Compute an approximate patch length b for the desired resonant frequency using $b = 0.49\lambda_0/\sqrt{\epsilon_r}$. Choose a patch width $a = 0.65\lambda_0/\sqrt{\epsilon_r}$. Choosing these patch dimensions will yield an aspect ratio of $a/b \approx 1.3$, which will help suppress higher order modes in the patch and will produce a patch that radiates with almost 100 percent efficiency. The parameter s is chosen to equal $w/2$ simply for practical reasons and does not appear explicitly in the model.

Parameter	*Dimension (inches)*
a	0.382
b	0.278
d	0.098
s	0.024

Table 4.1. Patch Antenna Dimensions

b. Make an initial guess at the real part of the patch edge impedance. This will be the same value as the impedance of the microstrip line feeding the patch. Compute the admittance of the main patch section Y_c.

c. Compute Δl and slot admittances $Y_{s1,s2}$.

d. Equation 4.1 is then iterated with successive values of b and d until the imaginary part of the input impedance is zero, and the real part of the input impedance is equal to the impedance of the microstrip feed line.

Table 4.1 lists the patch antenna dimensions used in the lens design. With the design of the patch antennas complete, the next step is to determine the path length equations for the lens.

4.2.2 Path Length Equations The geometry for a two-dimensional lens is shown in Figure 4.3. The lens has focal length F and arbitrary thickness W_0. Note that aperture antenna elements are displaced a distance r from the focal axis z and the feed antenna elements are displaced a distance ρ, where r and ρ are not necessarily the same distance. The feed- and aperture-side elements are connected by a transmission line of electrical length W. The following equations were derived for the general case of when the focal points are located at points $(y, z) = (-F\cos\theta_0, \pm F\sin\theta_0)$ off the focal axis [14]. The location of the feed side elements in terms of the aperture side elements is given by:

$$\rho = r\left[\frac{F^2 - r^2\sin^2\theta_0}{F^2 - r^2}\right]^{1/2} \tag{4.10}$$

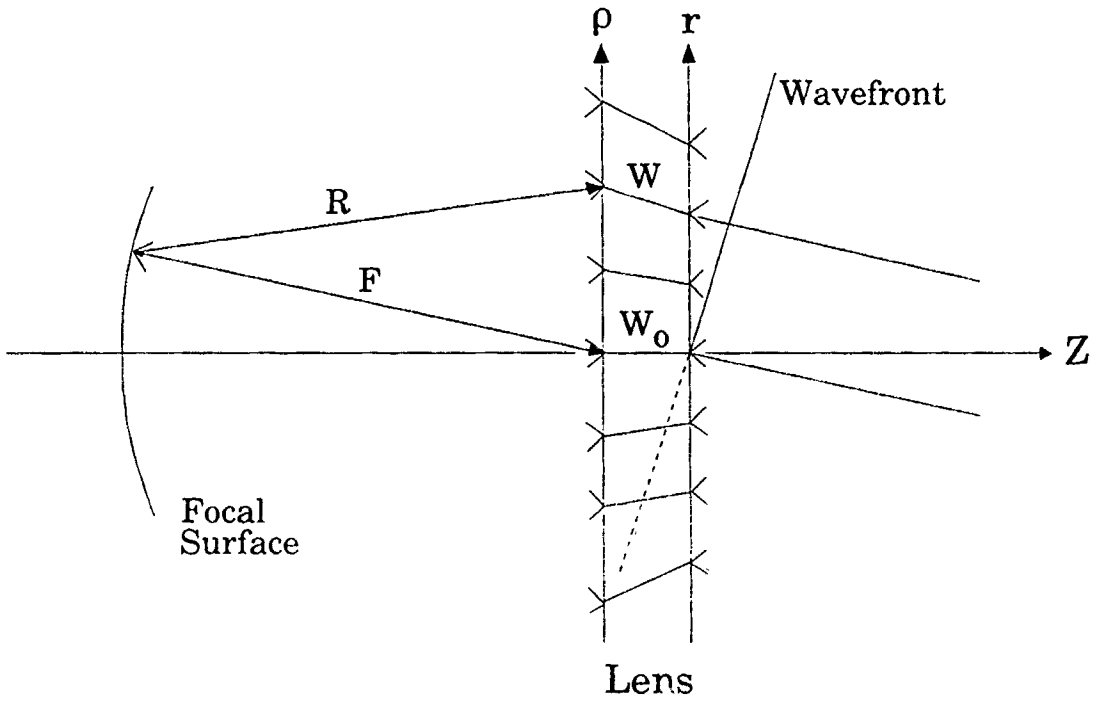

Figure 4.3. Geometry for the 2-D lens

The expression for the electrical line length W is then:

$$W = F + W_0 - \frac{1}{2}\left[F^2 + \rho^2 - 2\rho F \sin\theta_0\right]^{1/2} - \frac{1}{2}\left[F^2 + \rho^2 + 2\rho F \sin\theta_0\right]^{1/2} \quad (4.11)$$

This particular lens design uses two geometric degrees of freedom: the first in the length of transmission line connecting feed- and aperture-side elements; and the second in the different radial displacement of the aperture- and feed-side antenna elements. The second degree of freedom is applied in order to give the lens good wide angle focusing [6].

For a three dimensional lens design, Equations 4.10 and 4.11 remain the same, but r and ρ are now the radial coordinates for the aperture and feed sides respectively. In the 2-D case, r and ρ were the radial displacement along a linear axis, whereas in the 3-D case, they are the radial displacement throughout a plane. It is pointed out in [6] that for a three-dimensional lens design, the best choice for the focal angle is $\theta_0 = 0$, which will form a single on axis focal point. McGrath [2] states that this choice of focal angle will yield the largest scan region for any given maximum path length error. Path length error is a common indicator of the scanning performance of the lens. Therefore, a single on-axis focal point was chosen for the lens design.

4.3 Lens Fabrication

Lens fabrication followed the same three step procedure outlined in Chapter 3 for the prototype slot coupler fabrication. The only difference is that now we are working with hundreds of slot couplers, microstrip lines, and patch antennas. How we choose to lay out all these elements on the substrate will be an important part of the lens design process. One of the first things to decide in laying out a lens is choosing the array lattice for the aperture-side antenna elements. On one hand, we would like as wide an inter-element spacing as possible to help ease in the layout of patch antennas, microstrip transmission lines and slot couplers. However, since our lens will be scanned out to ± 30 degrees, grating lobes could be a problem if the inter-element spacing is too wide. For the lens design an equilateral triangular lattice with inter-element spacing of $0.74\lambda_0$ was selected for the aperture-side antenna elements. This was the spacing used in [2], and happens to be the lattice that yielded the widest inter-element spacing without the appearance of grating lobes in the ± 30 degree region. Feed-side antenna elements will then be a function of ρ as in Equation 4.10.

There are a total of 199 patch antennas on both the aperture and the feed sides of the lens.

Overall diameter of the aperture side of the lens was 15.4 inches as measured to the centers of the outermost elements. The diameter of the feed side array will be closer to 16.0 inches since feed-side elements are radially displaced outward from the aperture-side elements. The maximum size mask that could be generated at the photo lab was 17.0 inches and was the limiting value in the overall lens diameter. But even without this mask constraint, lens diameter was constrained to be less than 20 inches since the substrate selected was only available in 20 by 20 inch sheets. Overall, the lens is 0.10 inch thick and weighs about 4 pounds.

One significant change in this lens design over the two previous designs [2], [6] is the layout of the aperture-side elements relative to the feed-side elements. In [2] and [6] an aperture-side patch antenna would be connected to a feed-side patch which was located almost directly behind it (see Figures 2.2 and 2.3). This architecture resulted in several problems. First, microstrip lines were running too close to the radiating edge of the patch antennas, causing mutual coupling and interference between patch antennas and microstrip lines. Second, because of the cramped area in which to layout microstrip lines, slot couplers were crossing underneath microstrip lines at more than one point along the line.

In the new lens design, instead of an aperture-side element being connected to a feed-side element which is located directly behind it (refer to Figures 2.2 and 2.3), an aperture-side element is connected to a feed-side element that is located diagonally to it. The result is less competition for the same area in the layout of patch antennas, slot couplers, and microstrip lines.

Figure 4.4 shows how the new lens architecture would look. The drawing is shown to scale and represents how a typical aperture/feed-side antenna element is positioned on the lens, one patch antenna relative to the other. Also shown is the microstrip feed lines and slot coupler. Aperture- and feed-side patch antennas dimensions are listed in Table 4.1. The feed through slot is 0.03 by 0.346 inches. Keep in mind that the location of feed-side antenna elements and microstrip line lengths are a function of position on the lens, so that the relative distance between the patch antennas shown in Figure 4.4 will vary somewhat with each pair of antenna elements on the lens.

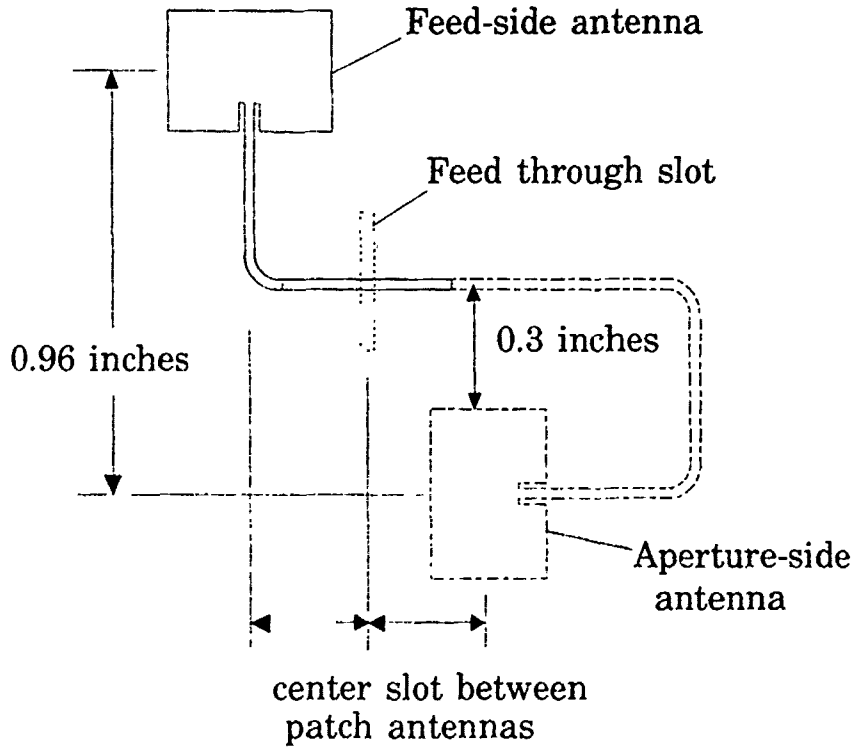

Figure 4-4. New Lens Architecture

In general, slots were located half way between the aperture-side and the connecting feed-side antenna element in the horizontal direction and about 0.3 inches above the feed-side elements in the vertical direction. The majority of the differential path length used in focusing the energy is accomplished in the microstrip lines on the aperture-side of the lens. Microstrip lines on the feed-side were almost of identical length, varying only enough to extend past the changing slot location.

A final change to the architectures of [2], [6] is the polarization of the lens. In the previous designs, both the aperture and feed side patch antennas were polarized in the same direction. This meant that the unfocused energy that was spilled over the lens was interfering with the focused energy coming through the lens. The result was a degradation in the radiation pattern. In the new design, feed-side antenna elements are cross-polarized to the aperture-side elements, the result is a better focused beam.

All microstrip lines were 0.0235 inches wide and a 90 degree bend of radius= 0.10 inches was used in the routing of all microstrip lines. Exactly three of these 90 degree bends (two on the aperture-side and one on the feed-side) were used throughout the lens in connecting each aperture/feed-side pair.

4.4 Testing

Lens testing was accomplished over a five day period at the Rome Laboratory antenna measurement facility, Ipswich MA. The facility has a 1/2-mile range with a 6 foot dish used as the transmitting antenna. The lens was mounted in the fixture shown in Figure 4.5. The fixture allows for the lens to be mounted solidly to the rotating positioner turntable, while the feed can be scanned up to ± 30 degrees off the axis of the lens. The feed can be also moved along the boom support to change focal length. During all pattern measurements, a shroud (lined with absorber) was placed over the region between the feed horn and the lens to prevent spillover and stray radiation that might corrupt pattern measurements.

4.4.1 Pattern Cuts The first measurements made on the lens were E-plane pattern cuts. It was discovered, after the E-plane patterns were taken, that the feed side antenna array elements were not mounted precisely in the center of the lens mounting fixture. This caused the feed horn to be positioned slightly off the focal point of the lens, resulting in a slightly defocused beam. This problem was

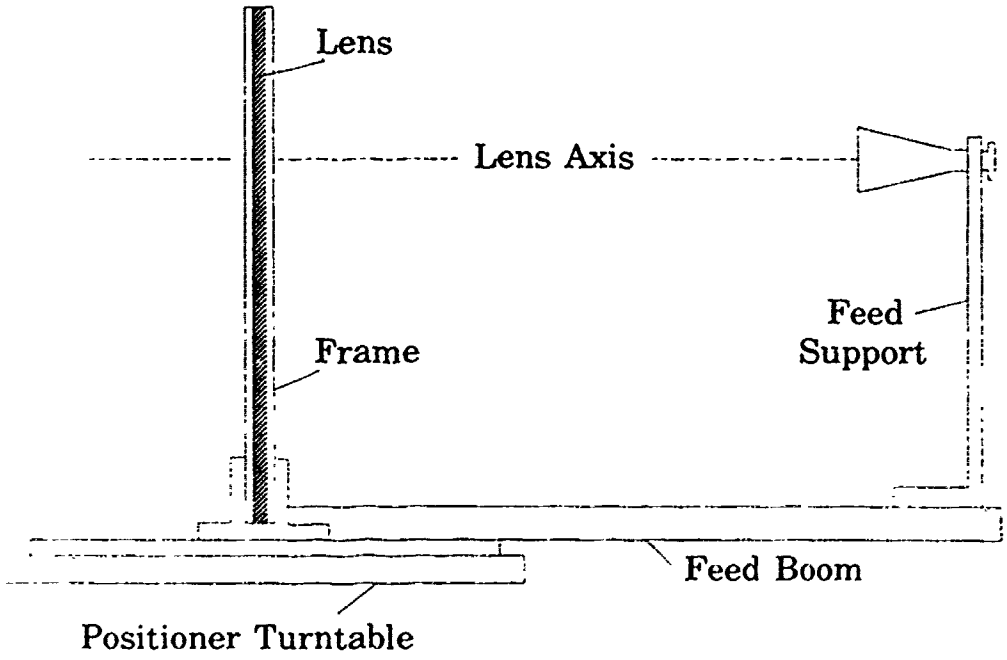

Figure 4.5. Lens Mounting Fixture

corrected before the H-plane measurements were made but there was not enough time to retake the E-plane patterns. Changing the set up between the E- and H-plane pattern cuts required removing the shroud, removing the lens from the fixture, rotating the lens, rotating the transmitter dish and then reassembling everything. All pattern cuts including the off-axis patterns were made with the feed located 40 inches from the lens. In other words, there was no refocusing of the feed as the feed was moved off-axis.

Figure 4.6 shows the measured E-plane pattern of the lens. The pattern is reasonably well focused as evidenced by the well shaped main beam, the depth of the first nulls and the symmetry of the first side lobes. A theoretical antenna pattern is shown in Figure 4.7 for comparison. The theoretical pattern was based on an array of 199 uniformly illuminated elements placed in a equilateral triangular grid with $0.74\lambda_0$ spacing. From this figure, it is seen that the array should have a half power beam width (HPBW) of 5.2 degrees and should have side lobe levels around -17 dB. The measured HPBW was 6.0 degrees and side lobe levels are in the 12-15 dB range. Broadening of the main beam is partially due to the edge taper and the de-focusing caused by the misalignment of the feed horn. E-plane patterns of the previous lens design are shown in Figure 4.8 for comparison. Keep in mind that a different feed horn (one with a higher gain) was used in the previous lens design so side lobe levels will be lower for the previous lens design. By comparing Figure 4.6 to Figure 4.8, it is seen that the radiation patterns are much more symmetric in the new lens design than in the previous lens design. First side lobe levels are about 3 dB apart in the new lens design, whereas they are about 16 dB apart in the previous lens design. As the beam is scanned off-axis in the previous design, even the main beam starts to become distorted. It should be pointed out that in the previous lens testing, the lens was refocused as the feed was moved to the various scan angles and should result in a better focused pattern than a lens that was not refocused. In the following radiation patterns the lens was not refocused at the different scan angles but still achieved as good a pattern as the previous lens design with refocusing. It is felt that the improved patterns are due to the increased spacing between the microstrip transmission lines and the radiating edge of the patch antennas. Also, by increasing the efficiency of the feedthrough, there is most likely result in less stray radiation emanating the feedthrough point.

Figures 4.9, 4.10, and 4.11 show the E-plane cuts of the lens with the feed

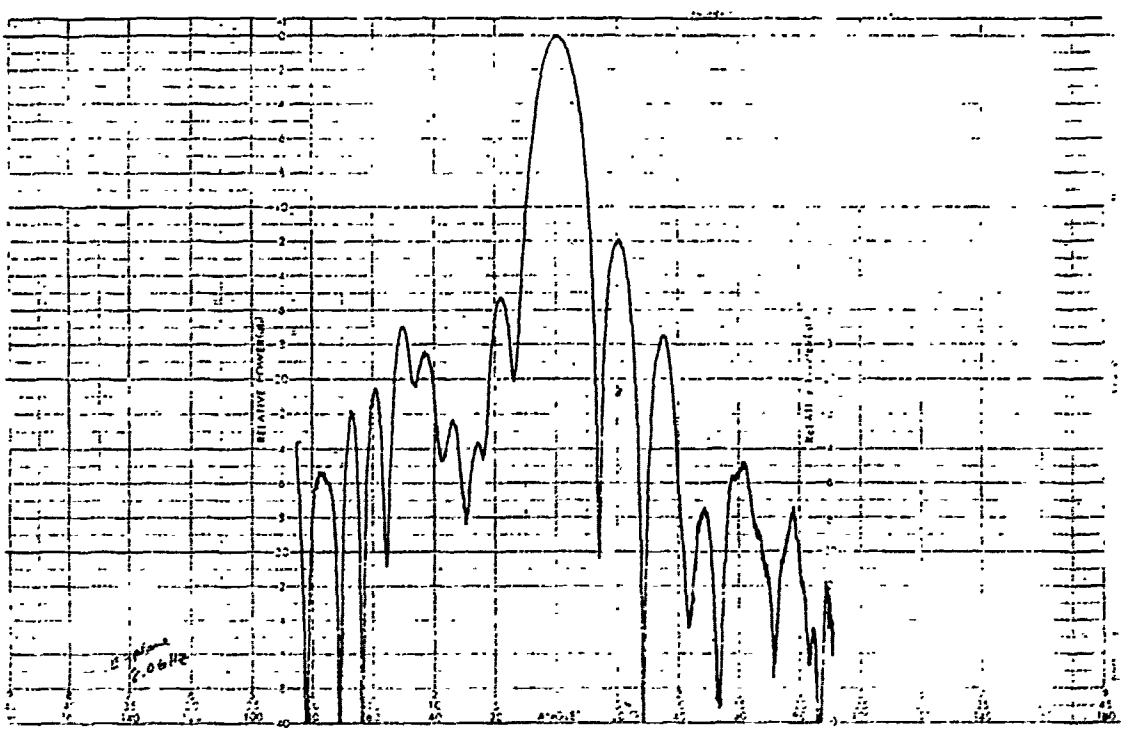

Figure 4.6. E-Plane Cut, 8.0 Ghz. On-axis

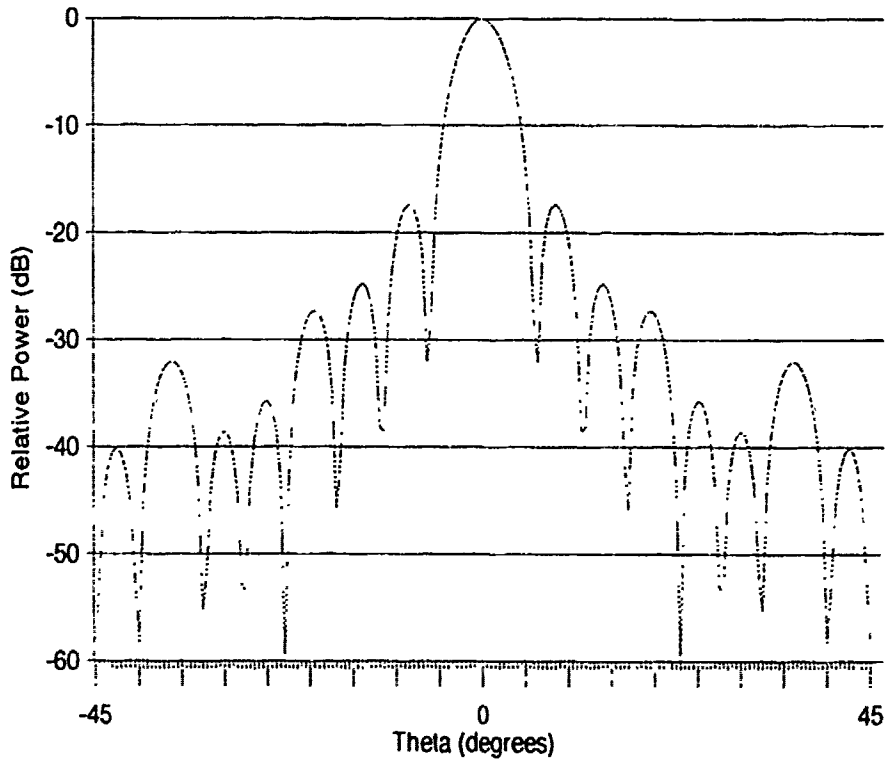

Figure 4.7. Theoretical Antenna Pattern, 8.0 GHz, $0.74\lambda_0$ Spacing

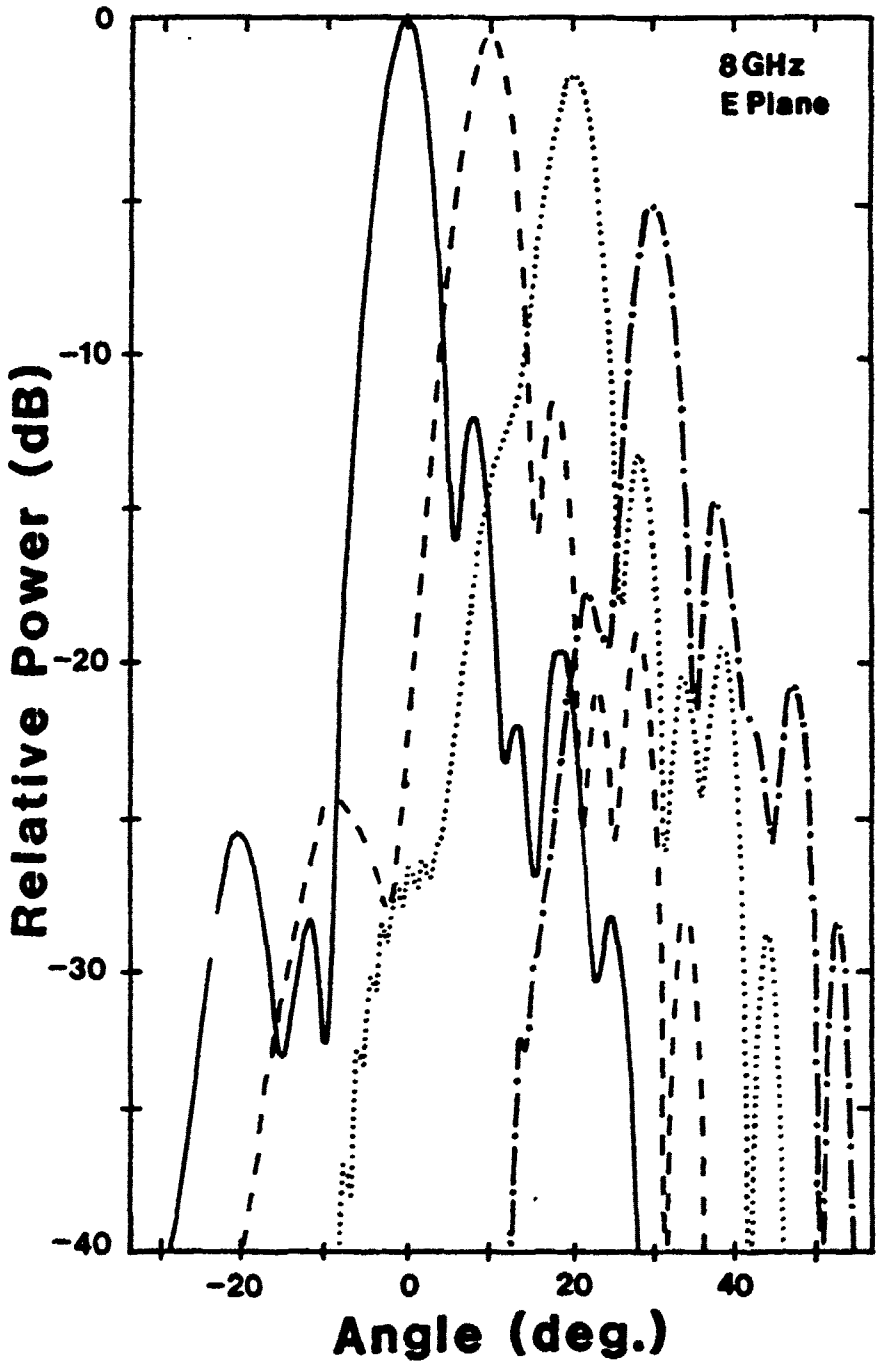

Figure 4.8. E-Plane Patterns from Previous Lens [2]

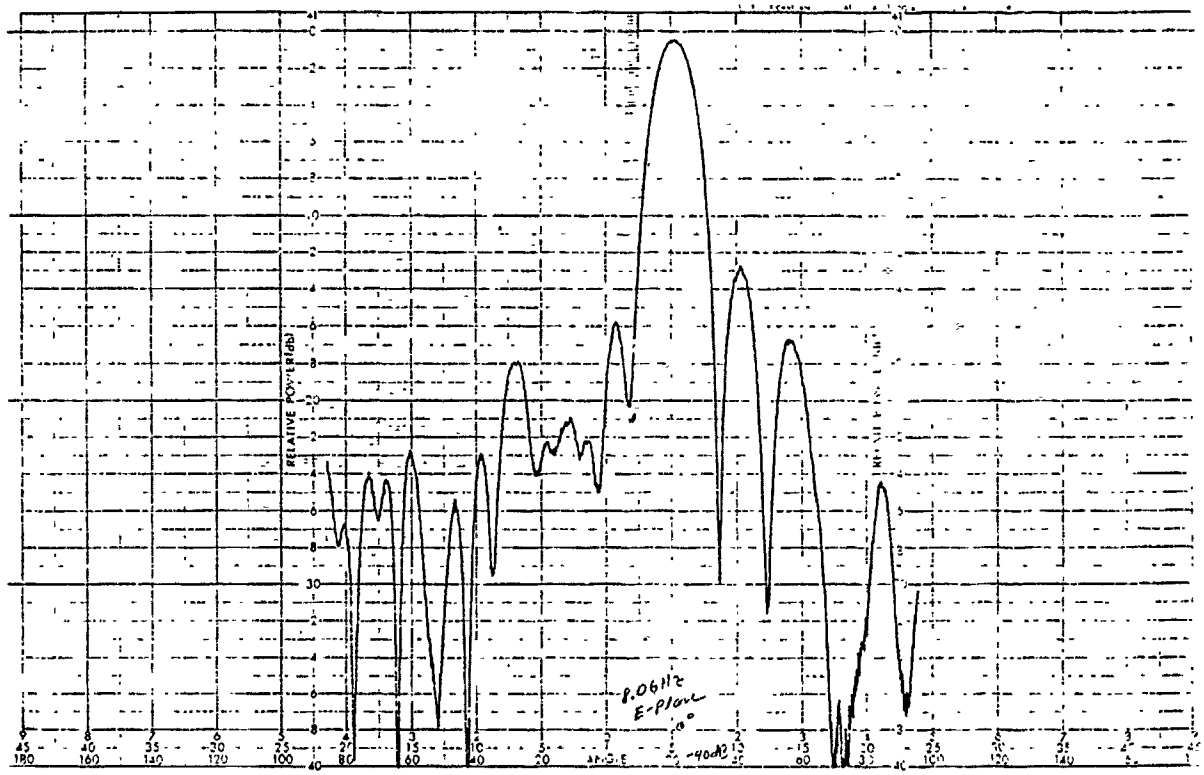

Figure 4.9. E-Plane Cut, 8.0 GHz, 10 Degree Scan

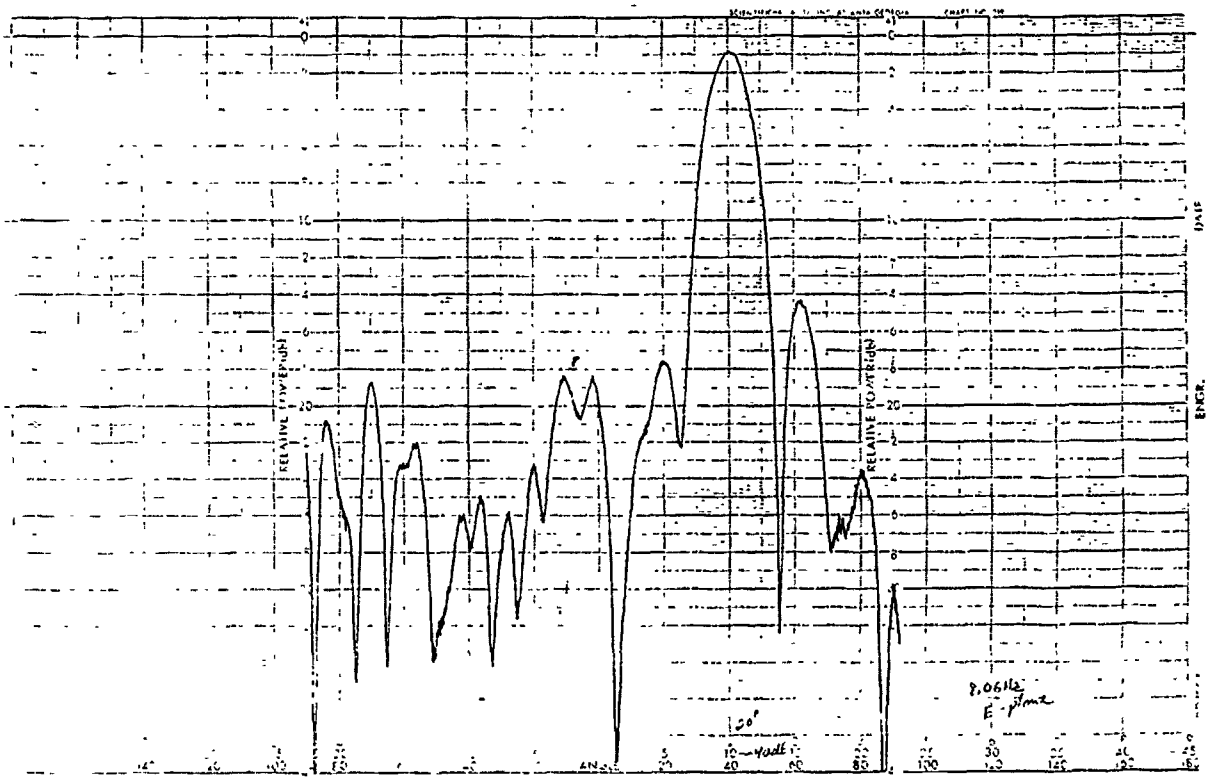

Figure 4.10. E-Plane Cut, 8.0 GHz. 20 Degree Scan

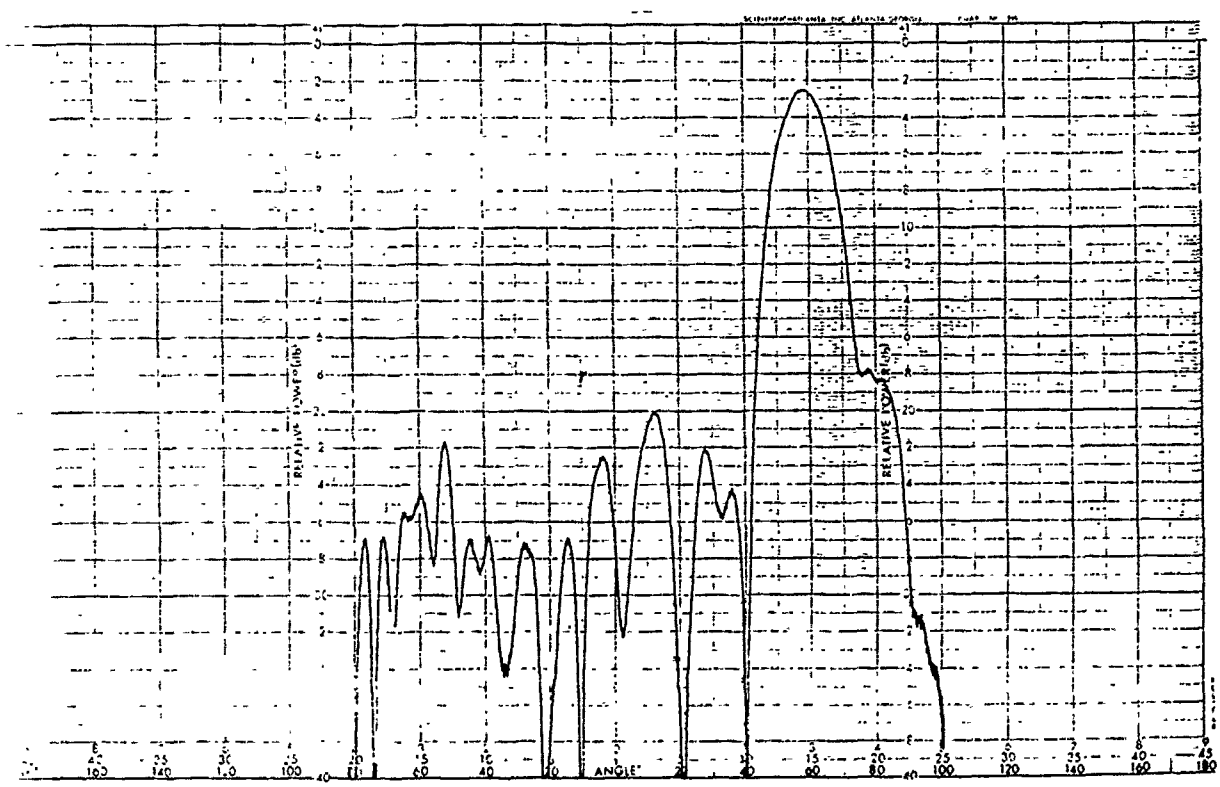

Figure 4.11. E-Plane Cut, 8.0 Ghz. 30 Degree Scan

moved off-axis by 10, 20 and 30 degrees respectively. Note there is a slight decrease in antenna gain and a slight broadening of the main beam as the feed is scanned. The usual $cos\theta$ scanning loss is contributing to this gain decrease. In Figures 4.9 and 4.10 it can be seen that the main beam remains well shaped and that first nulls remain deep. First side lobe levels remain about 3 dB apart, the same as the on-axis pattern. In the 30 degree scan shown in Figure 4.11, the main beam remains well shaped, but one of the first nulls is smeared out by the first side lobe. This can be expected since the feed was not refocused as in [2] and [6]. It should be noted that a lens that is not refocused will exhibit a pattern that becomes progressively more defocused as the feed is moved away from the focal point. The result is a pattern with filled in pattern nulls and asymmetric side lobes. Also with the feed moved to the 30 degree position, the feed horn was getting close to the shroud wall, which may be interfering somewhat with the pattern. It will be seen later in the H-plane patterns that this problem was corrected when the shroud was reassembled for the H-plane cuts.

An on-axis H-plane pattern cut is shown in Figure 4.12. Here it is seen that the main beam is well shaped, the first nulls are deep, and the first side lobes are symmetric. Note also that the HPBW is about 5.2 degrees which, as already mentioned, was expected for an array of this size. Overall, the beam is better focused than in the E-plane. First side lobes are however higher than expected and far out nulls and side lobes are filled in and smeared. It is not known for sure what is causing the high side lobes. Some possibilities are: 1) a non-uniformly illuminated array, resulting from incorrect phasing/weighting to the array elements, and 2) stray radiation from sources other than antenna elements (such as slot couplers or open-ended microstrip lines). Further testing would be required to isolate if the cause of the higher side lobes were from stray radiation from slot couplers, open-ended microstrip lines or the incorrect phasing of antenna elements. H-plane patterns of the previous lens design are shown in Figure 4.13 for direct comparison.

H-plane patterns for the lens scanned to 10, 20 and 30 degrees are shown in Figures 4.14, 4.15 and 4.16 respectively. For all scan angles, the main beam remains well formed and the first nulls remain deep. Side lobe levels do not seem to follow any particular pattern as the beam is scanned. On-axis, the side lobes are fairly even and symmetric. The side lobes then become uneven and asymmetric at the 10 and 20 degree scans and are then again even and symmetric at the 30 degree scan. Again

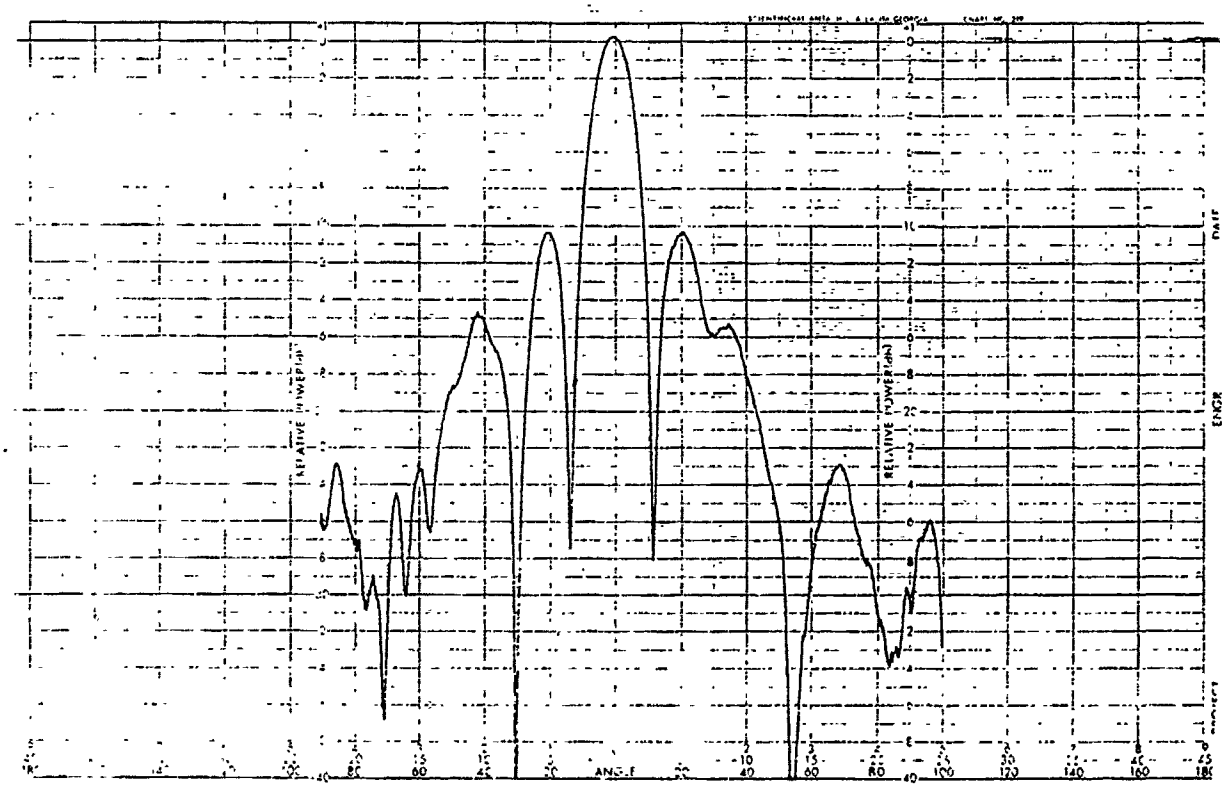

Figure 4.12. H-Plane Cut, 8.0 GHz, On-axis

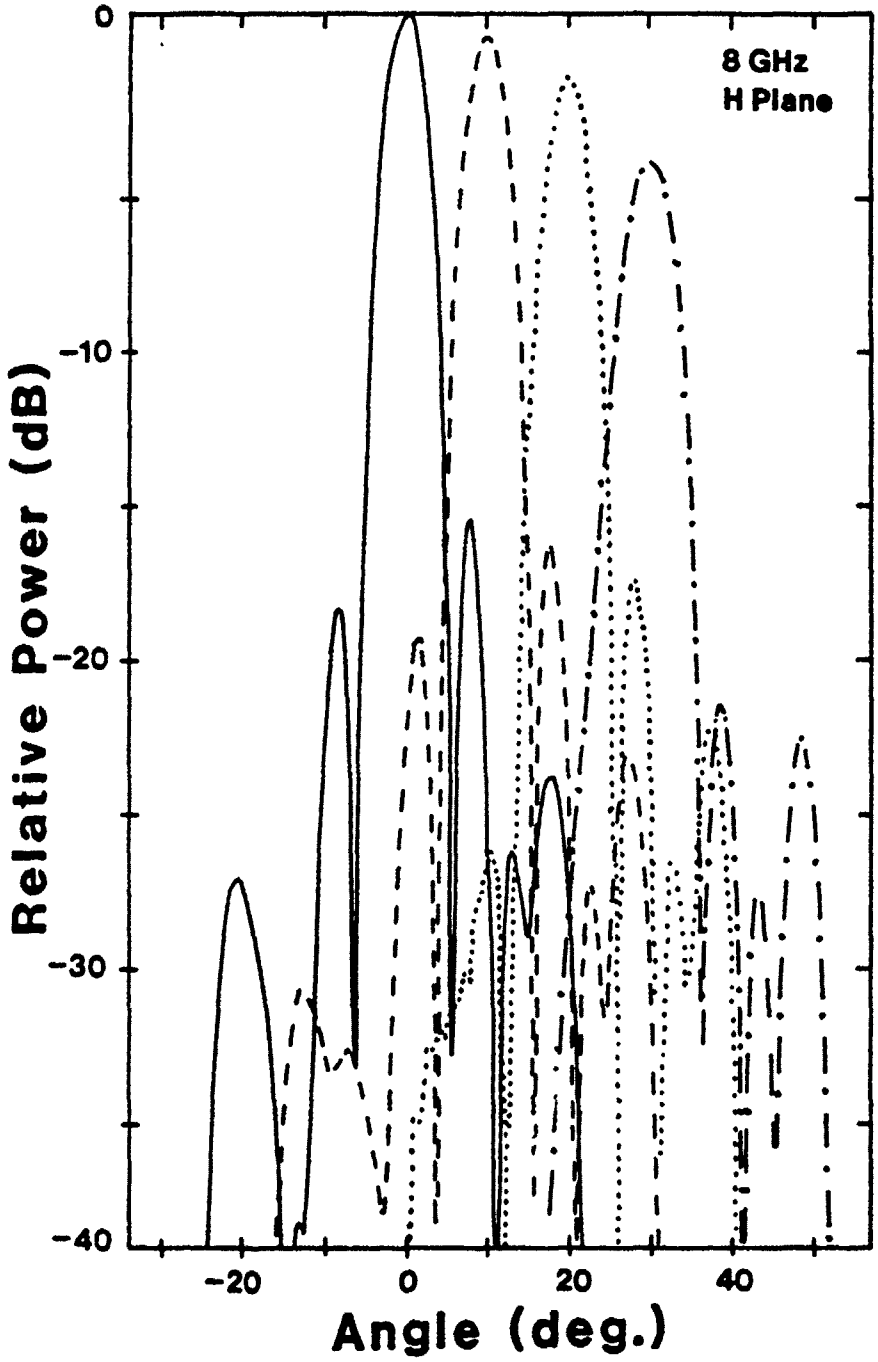

Figure 4.13. H-Plane Patterns from Previous Lens [2]

there is a gain decrease as the beam is scanned. Also note that the degradation seen in Figure 4.11, which was thought to be caused by the shroud, is not present in the 30 degree scan since the shroud was moved further away from the feed horn for the H-plane patterns cuts.

4.4.2 Lens Efficiency Lens efficiency was calculated using the following method. First, a maximum theoretical aperture gain was determined based on a uniformly illuminated array with the same diameter as the lens. In this case the lens diameter is 15.4 inches. Second, spillover loss was subtracted from this gain value since spill over energy represents energy that the lens cannot focus. Taper loss is also subtracted since the lens is not uniformly illuminated. The result of these first few steps is then the maximum theoretical gain that the lens could achieve if it were 100 percent efficient. The difference between this maximum theoretical gain and the actual measured gain represents loss in the lens.

Using the above procedure, the maximum theoretical aperture gain is then:

$$G = 4\pi \frac{D^2}{\lambda_0^2} \tag{4.12}$$

or 31.6 dB for a 15.4 inch aperture at 8.0 GHz. Spillover loss was determined by integrating over the feed horn patterns which are shown in Figures 4.17 and 4.18. The feed horn had a 2.125 by 2.875 inch rectangular aperture with a parabolic shaped flare to it. To make integration easier, the feed horn patterns were approximated as a rotationally symmetric $\cos^{15}\theta$ pattern. The following equations were used in the calculation of spillover [1]:

$$P(apert) = 2\pi \int_0^{\theta_h} P_H(\theta) \sin\theta d\theta \tag{4.13}$$

$$P(spill) = 2\pi \int_{\theta_h}^{\pi/2} P_H(\theta) \sin\theta d\theta \tag{4.14}$$

$$\%(spillover) = \frac{P(spill) \times 100}{P(aperture) + P(spill)} \tag{4.15}$$

where θ_h is the angle subtended from the lens axis to the edge of the aperture with its vertex at the focal point. The result of this calculation was a spillover loss of 6.0 dB.

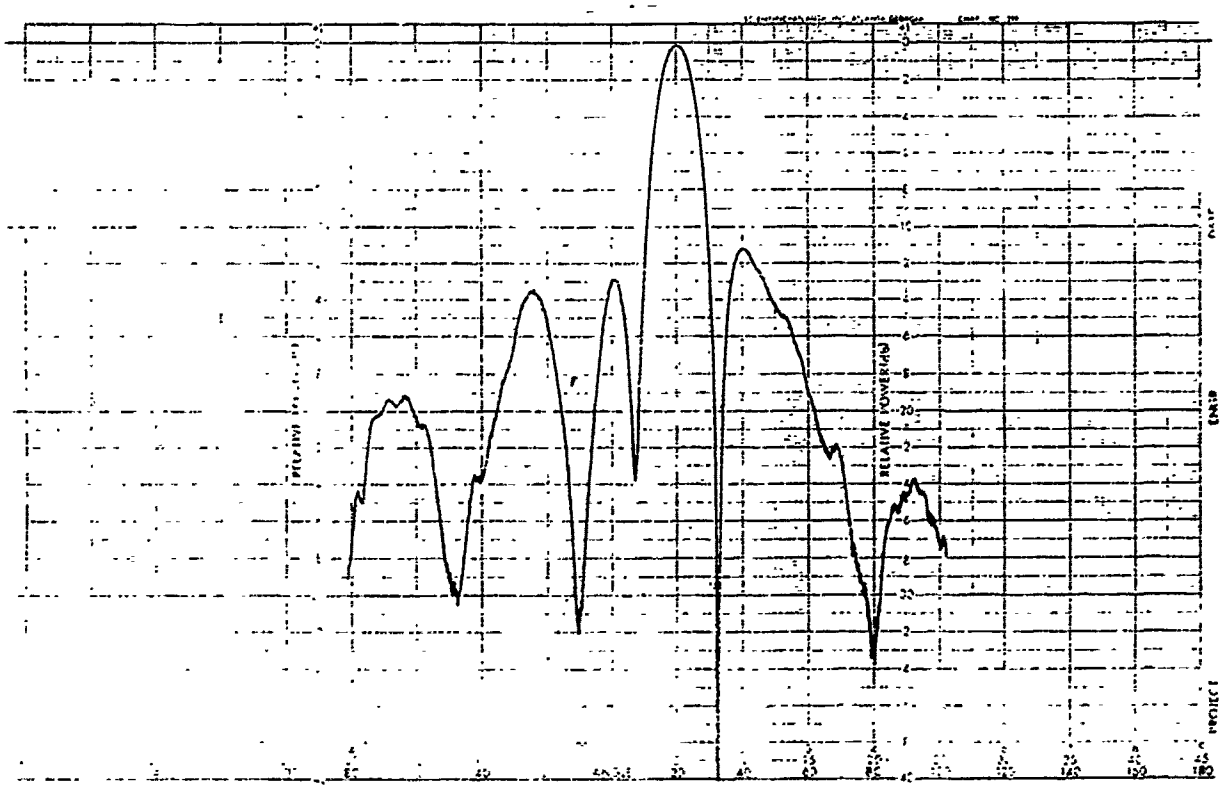

Figure 4.14. H-Plane Cut, 8.0 GHz, 10 Degree Scan

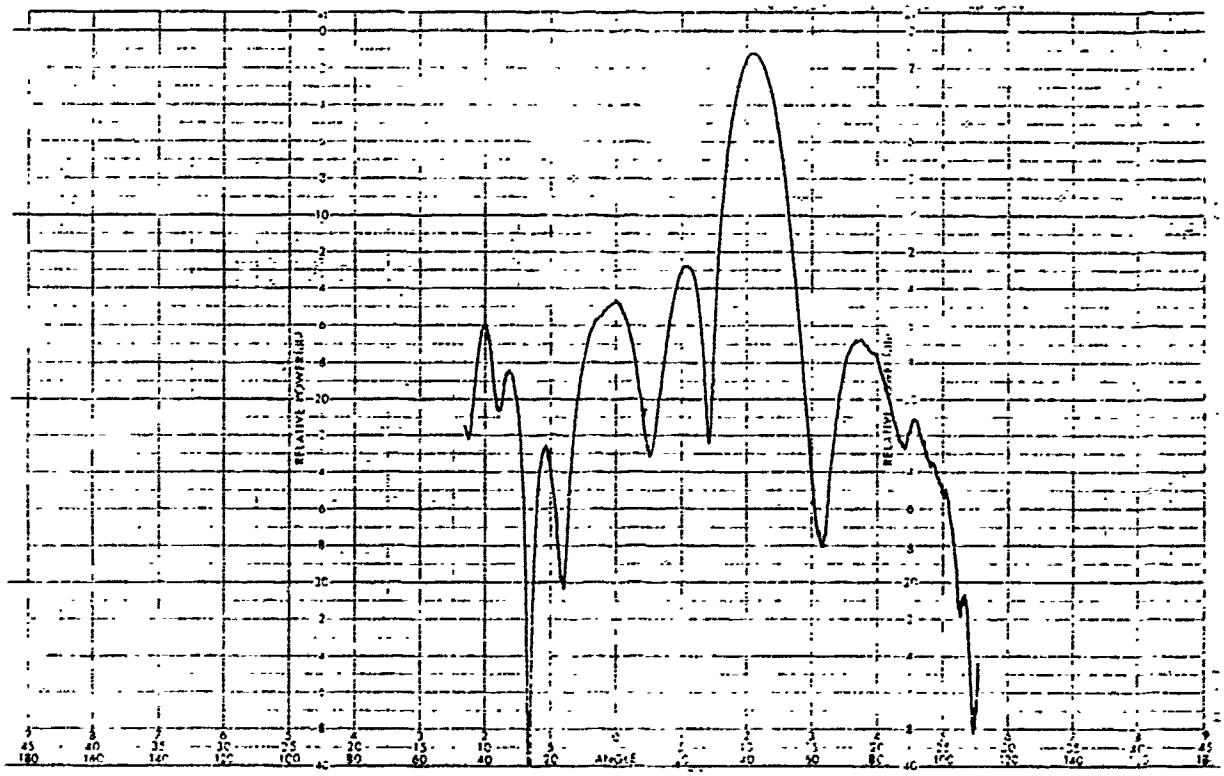

Figure 4.15. H-Plane Cut, 8.0 GHz. 20 Degree Scan

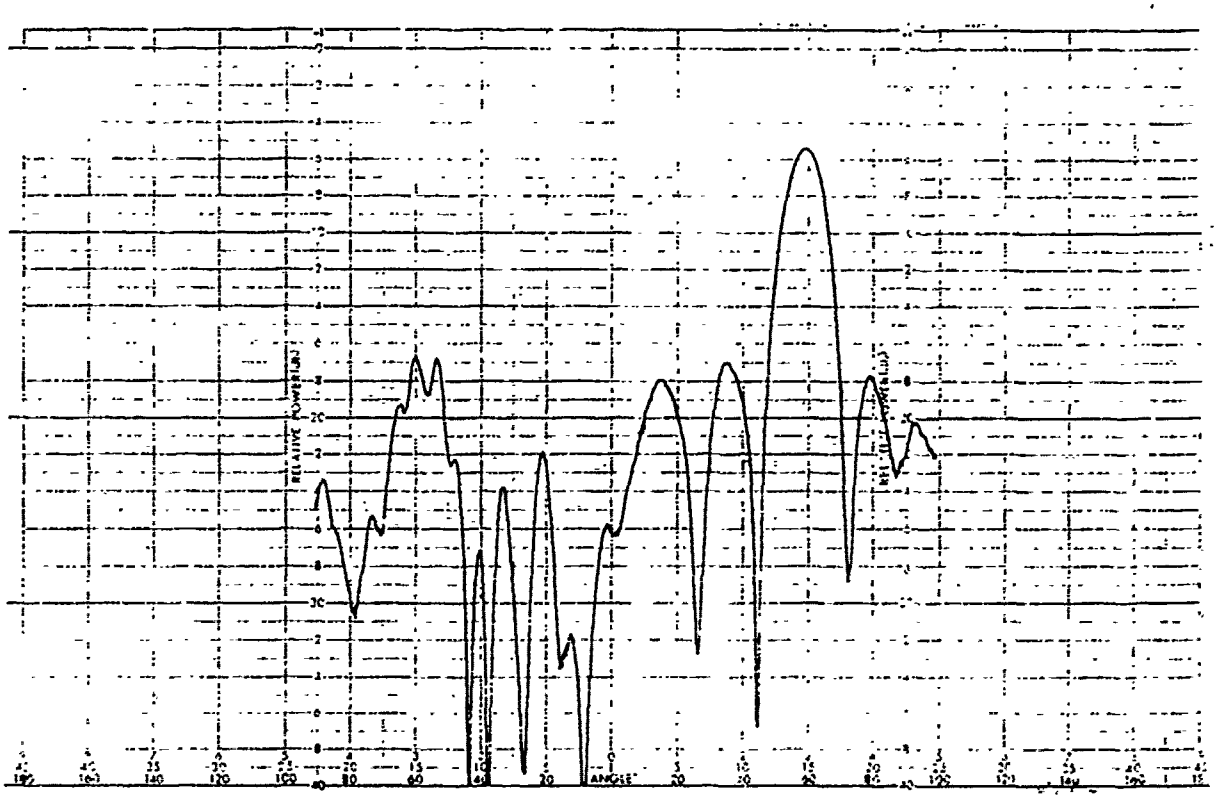

Figure 4.16. H-Plane Cut, 8.0 Ghz, 30 Degree Scan

Radial Distance (wavelengths)	*Weight*
center	1.000
0-0.74	0.994
0.75-1.48	0.978
1.47-2.21	0.950
2.22-2.96	0.914
2.97-3.70	0.869
3.71-4.44	0.818
4.45-5.22	0.795

Table 4.2. Array Element Weighting

Taper loss was determined by plotting the array pattern for a 199 element weighted planar array and noting the decrease in gain as compared with that of a uniformly illuminated array. A $0.74\lambda_0$ spacing was used in the array. Table 4.2 shows the weighting of each element according to radial distance from the center of the array in free space wavelengths.

The result was a 0.8 dB taper loss. Maximum theoretical gain for the lens is then 24.8 dB. Actual measured gain for the lens was 22.3 dB. Therefore, the lens has 2.5 dB of loss associated with it, which yields an overall lens efficiency of 56 percent. Since it is known from the insertion loss measurements of Chapter 3 that the maximum insertion loss through the slot coupler and microstrip line is less than 1.6 dB, there must be at least 0.9 dB of surface reflection in the lens. Surface reflection is a result of microwave energy being reflected at the lens/free space boundary. In future lens designs, the reduction of surface reflection should be one means explored to further improve lens efficiency.

A lens efficiency of 56 percent is a substantial increase over the previous lens designs [2], [6] which had efficiencies in the range of 15-31 percent. Two major factors account for the improved efficiency. First, a low-loss substrate was used instead of the lossy epoxy-fiberglass material used in [2], [6]. The result is reduced attenuation in the microstrip transmission lines. Second, an improved feedthrough slot coupler design resulted in less reflected energy at the microstrip-slot-microstrip transition point.

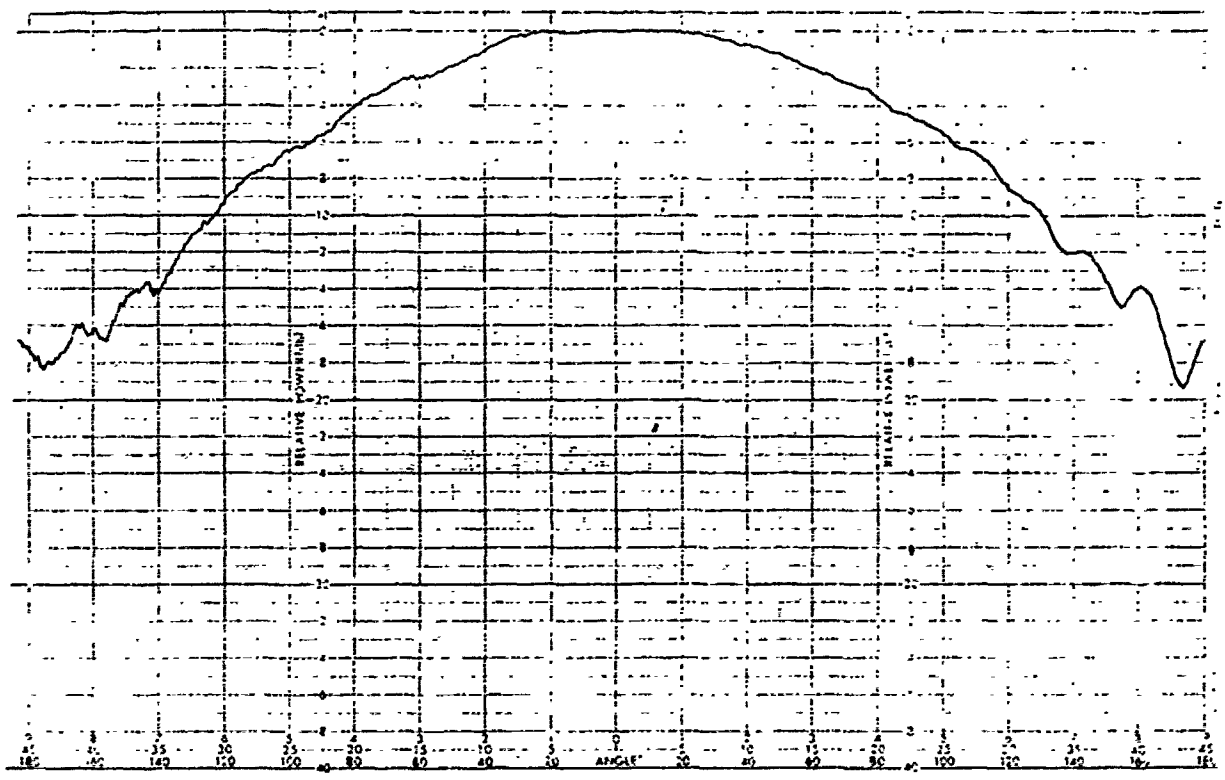

Figure 4.17. E-Plane Cut, 8.0 GHz, Feed Horn

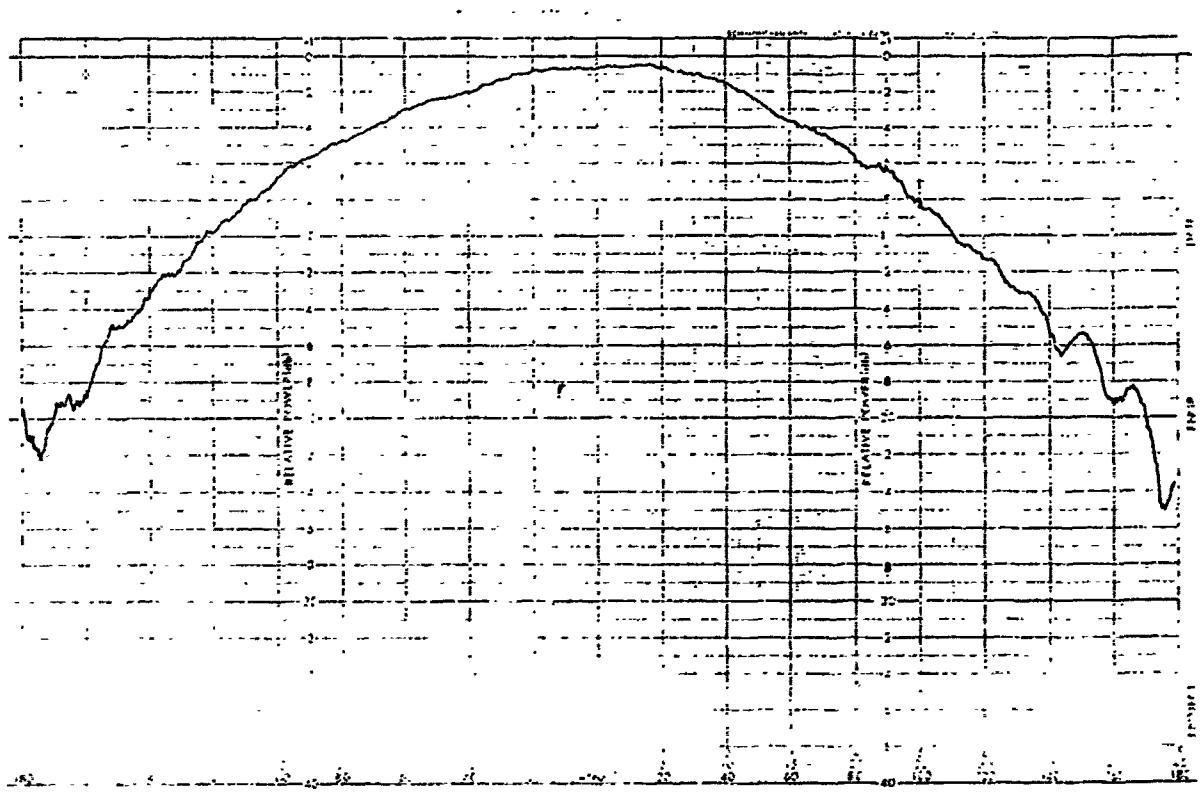

Figure 4.18. H-Plane Cut. 8.0 Ghz, Feed Horn

4.5 Conclusion

A lightweight, planar microwave lens was successfully designed, fabricated and tested. Testing of the lens demonstrated that the lens could scan a beam out to ±30 degrees in both the azimuth and elevation planes with acceptable pattern degradation. Lens patterns were then compared to previous lens designs where it was determined that the new lens architecture resulted in improved pattern cuts. It is felt that the improved patterns were due primarily to the reduction of stray radiation emanating from the feedthrough points and less interference between patch antennas, slot couplers, and microstrip lines.

Overall lens efficiency was demonstrated to be 56 percent. This is a 25 percent increase over previous planar lens designs. Two major factors account for the improved efficiency. First, a low-loss substrate was used which reduced the attenuation in the microstrip transmission lines. Second, an improved feedthrough slot coupler design resulted in less reflected energy at the microstrip-slot-microstrip transition point. Future lens designs may be able to achieve even higher lens efficiencies through the reduction of surface reflections which accounted for at least 0.9 dB of the loss in the lens.

V. *Conclusions and Recommendations*

5.1 Conclusions

A lightweight, planar microwave lens was successfully designed, fabricated, and tested. An 8.0 GHz, ten wavelength lens was only 0.1 inch thick and weighed less than 4 pounds. The lens should find many applications where a reduction in weight is of prime importance. It was demonstrated that the lens could scan a beam over a ±30 degree region in both the azimuth and elevation planes with acceptable pattern degradation. Overall, lens efficiency was measured at 56 percent. This is a 25 percent improvement over previous lens designs. Two factors contributed to the improved efficiency. The first factor was an improved slot coupler design. By reducing the reflections at the microstrip-slot-microstrip transition, more energy is being coupled to the second microstrip line, resulting in higher efficiency and less stray radiation from the feedthrough point. The second factor was the use of a low-loss dielectric substrate material in lens fabrication. Using a low-loss substrate resulted in reduced attenuation in the microstrip line. It was determined that surface reflection accounted for at least 0.9 dB of the loss in the lens.

A new lens architecture was used in this thesis in which aperture- and feed-side antenna elements were located diagonal to each other. The result was a layout in which lens elements such as patch antennas, slot couplers and microstrip lines were not spaced as closely together on the substrate as in previous lens designs. When these elements are placed close together, as in previous designs, interference takes place and a degradation in radiation pattern results. A notable improvement in beam quality was evident with the new architecture as a result of the increased spacing.

This is the first time that a model for the microstrip-slot-microstrip transition has been documented. The model worked well for some slot couplers that were fabricated but was off by as much as 1.9 dB on one other slot coupler that was tested. It was concluded that the model should be used in base line designs only until a better model is found Measurements on the slot couplers suggest that a slot with an electrical length of $0.400\lambda_s - 0.440\lambda_s$ seems to be the optimum choice in terms of insertion loss for a microstrip-slot-microstrip transition.

5.2 Recommendations

A better model for the microstrip-slot-microstrip transition is needed. Loss in the slot coupler could be reduced with either a better slot coupler model or second iteration prototype testing

Future lens designs should take into account surface reflections as one means to achieve a higher lens efficiency. This can be accomplished by actively matching the patch antennas in an array environment.

Further testing of the lens would be required to determine if the higher sidelobes observed in the radiation patterns were caused by incorrect phasing to the aperture antenna elements or stray radiation emanating from slot couplers and open-ended microstrip lines.

Appendix A.

This appendix contains the insertion loss measurements from the prototype slot couplers fabricated in Chapter 3.

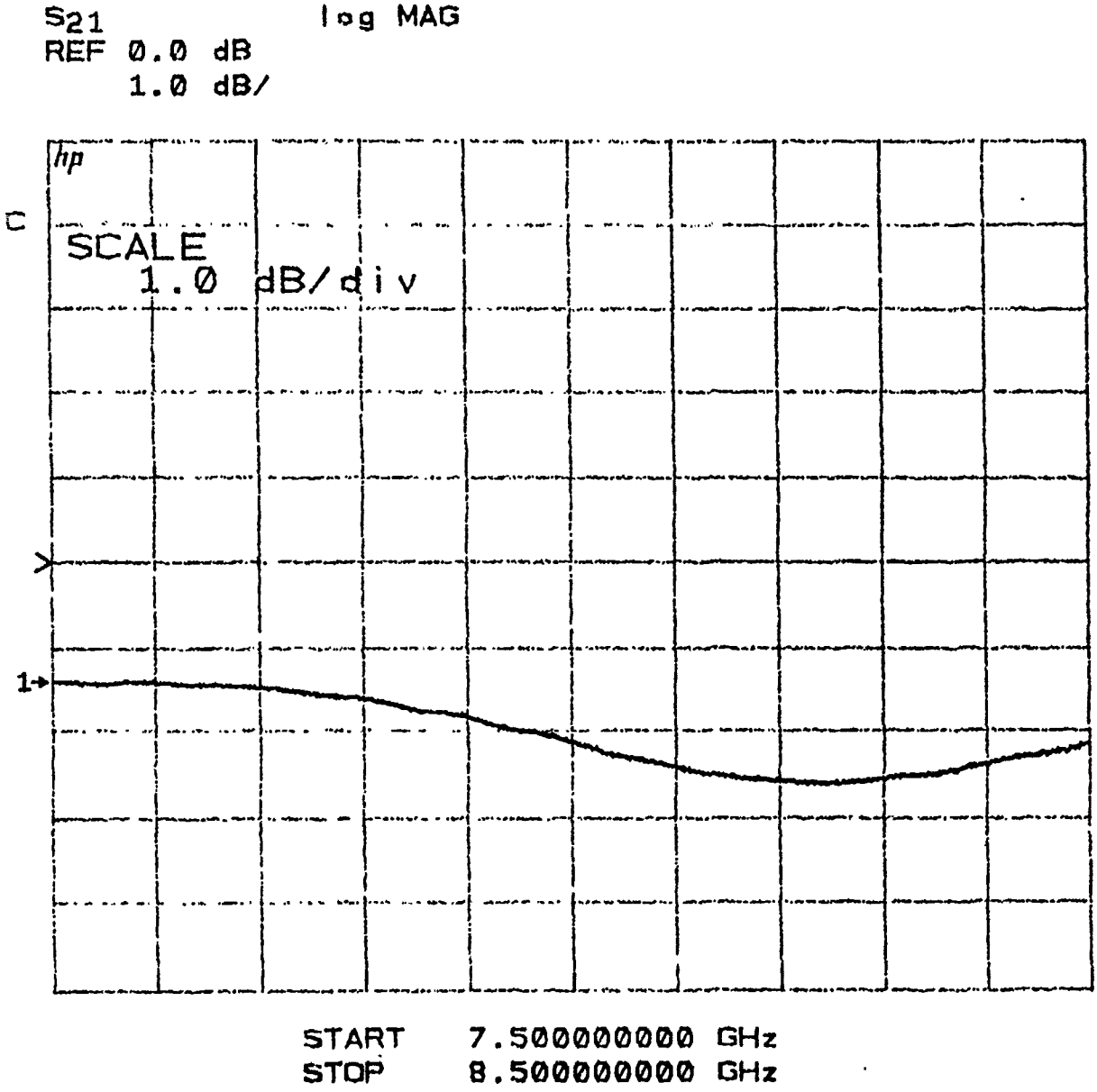

Figure A.1. Insertion Loss, SL=0.390 Inches, SW=0.03 Inches

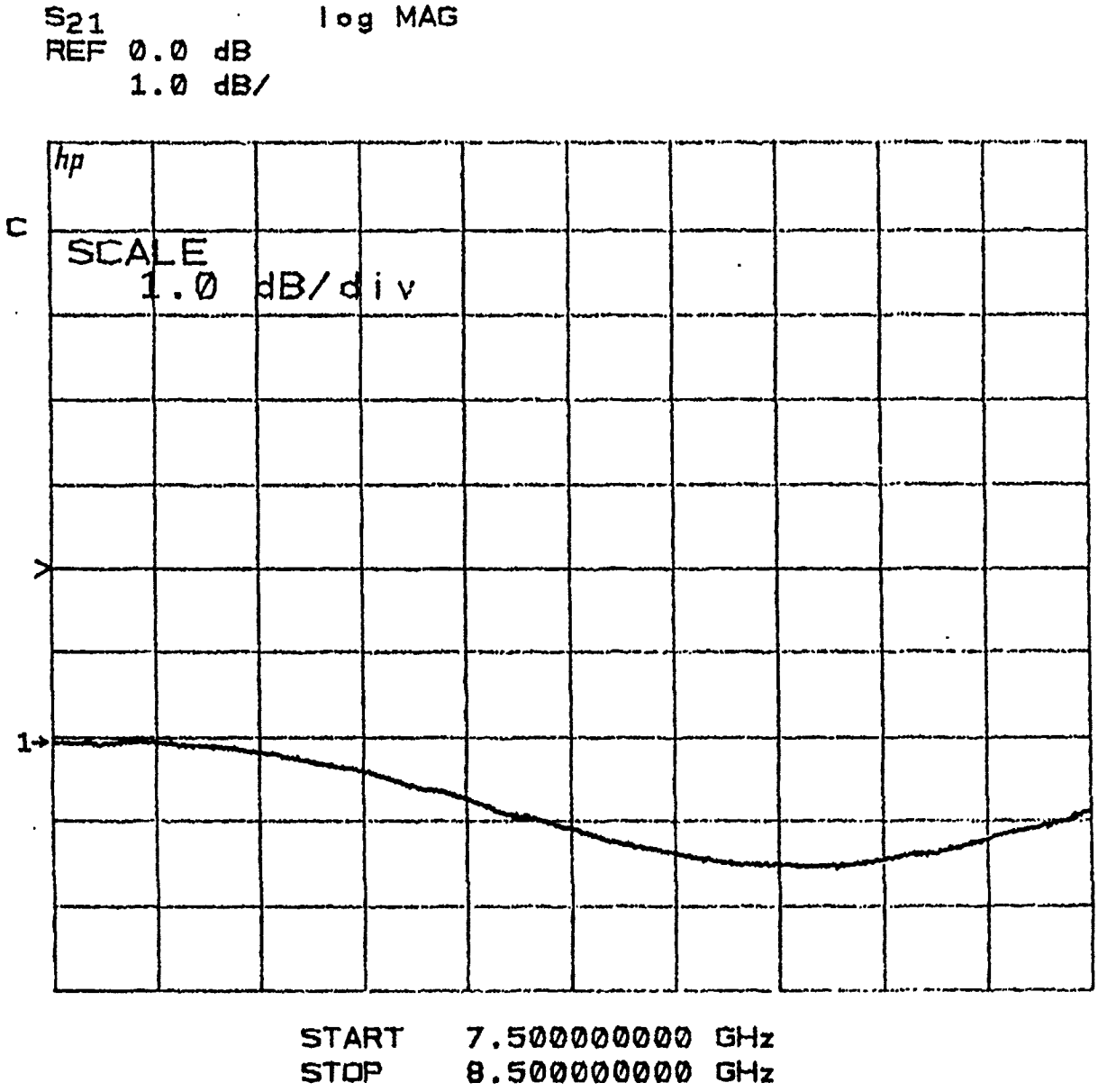

Figure A.2. Insertion Loss, SL=0.433 Inches, SW=0.03 Inches

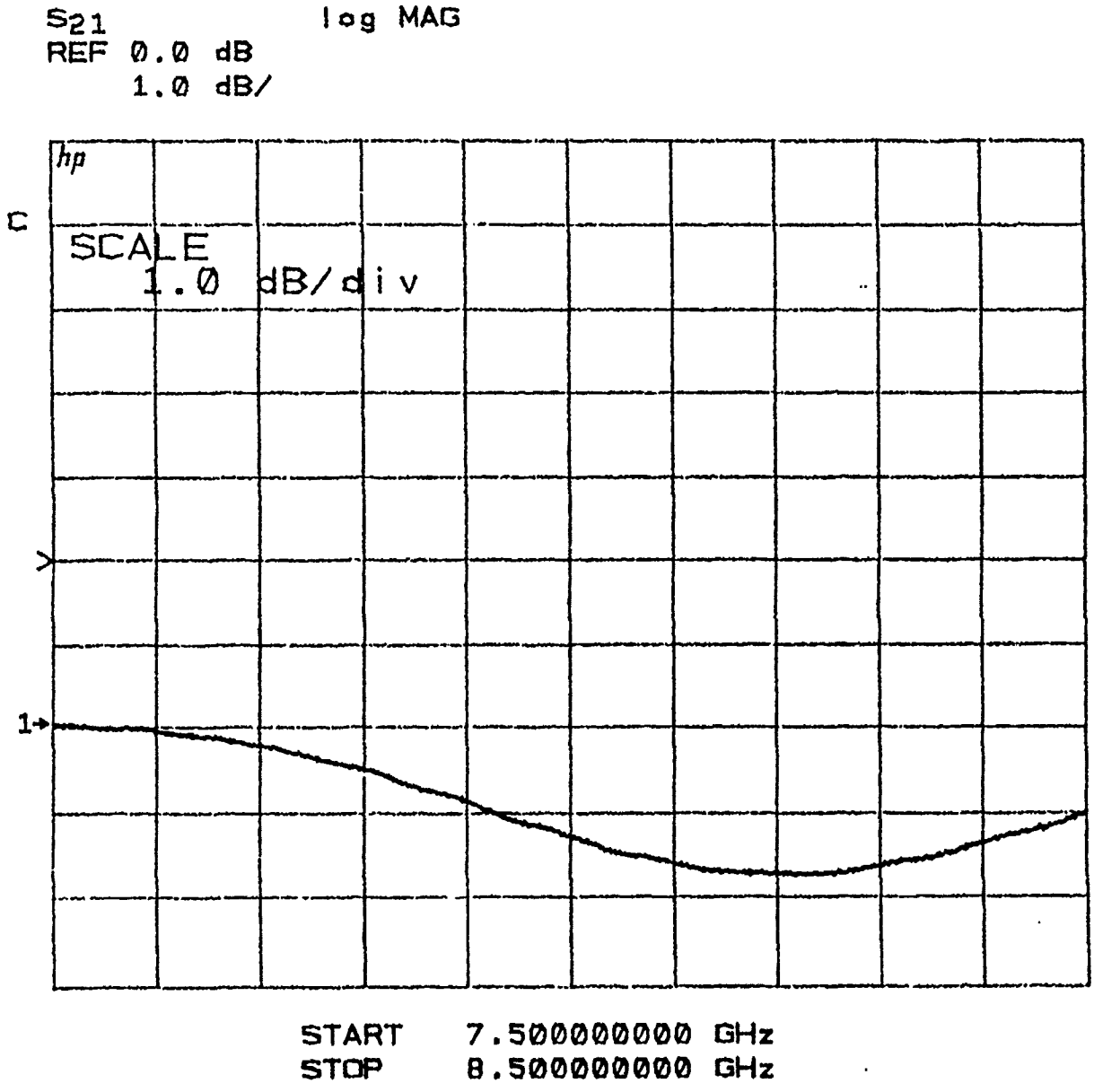

Figure A.3. Insertion Loss, SL=0.425 Inches, SW=0.02 Inches

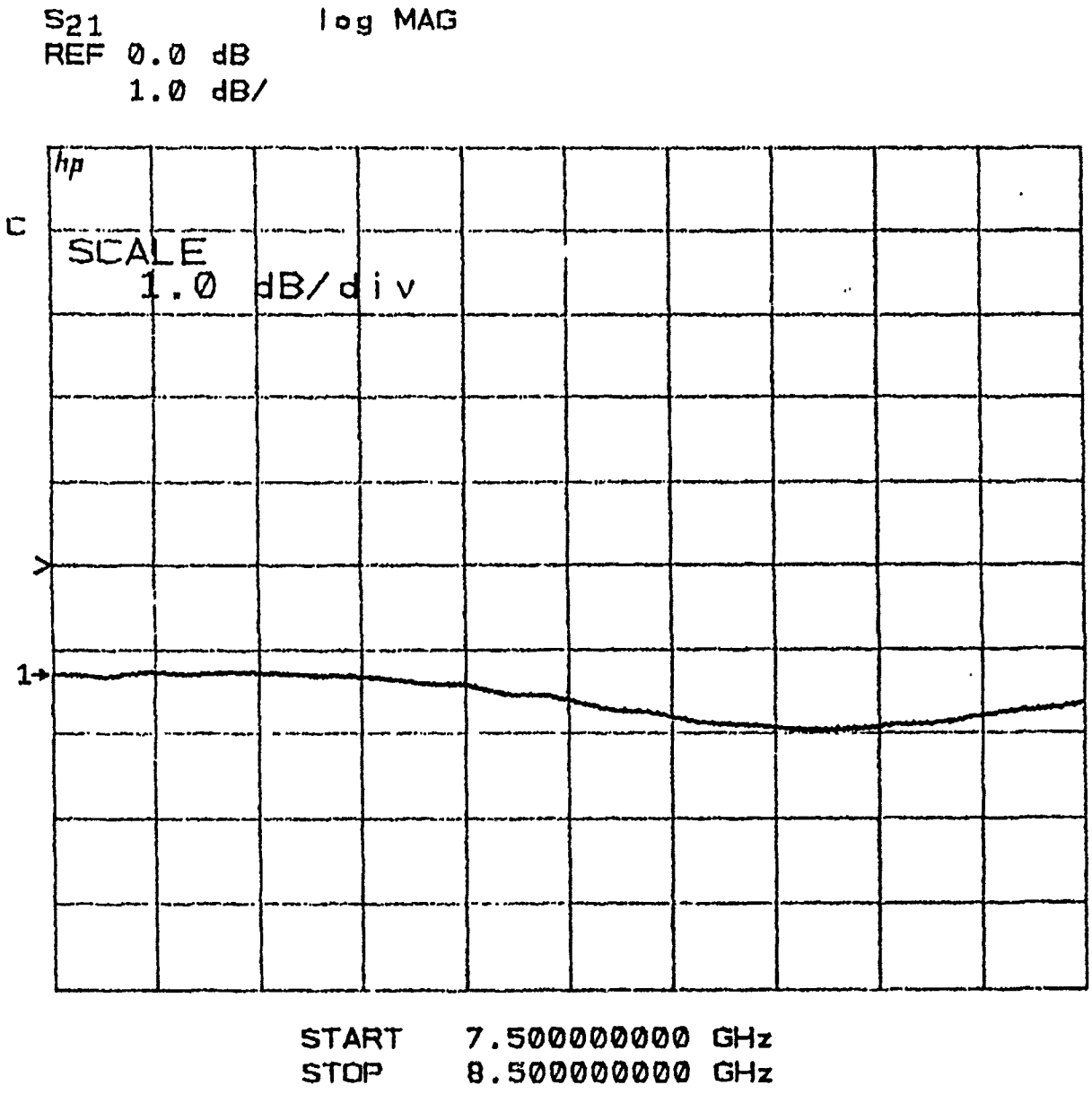

Figure A.4. Insertion Loss, SL=0.340 Inches, SW=0.02 Inches

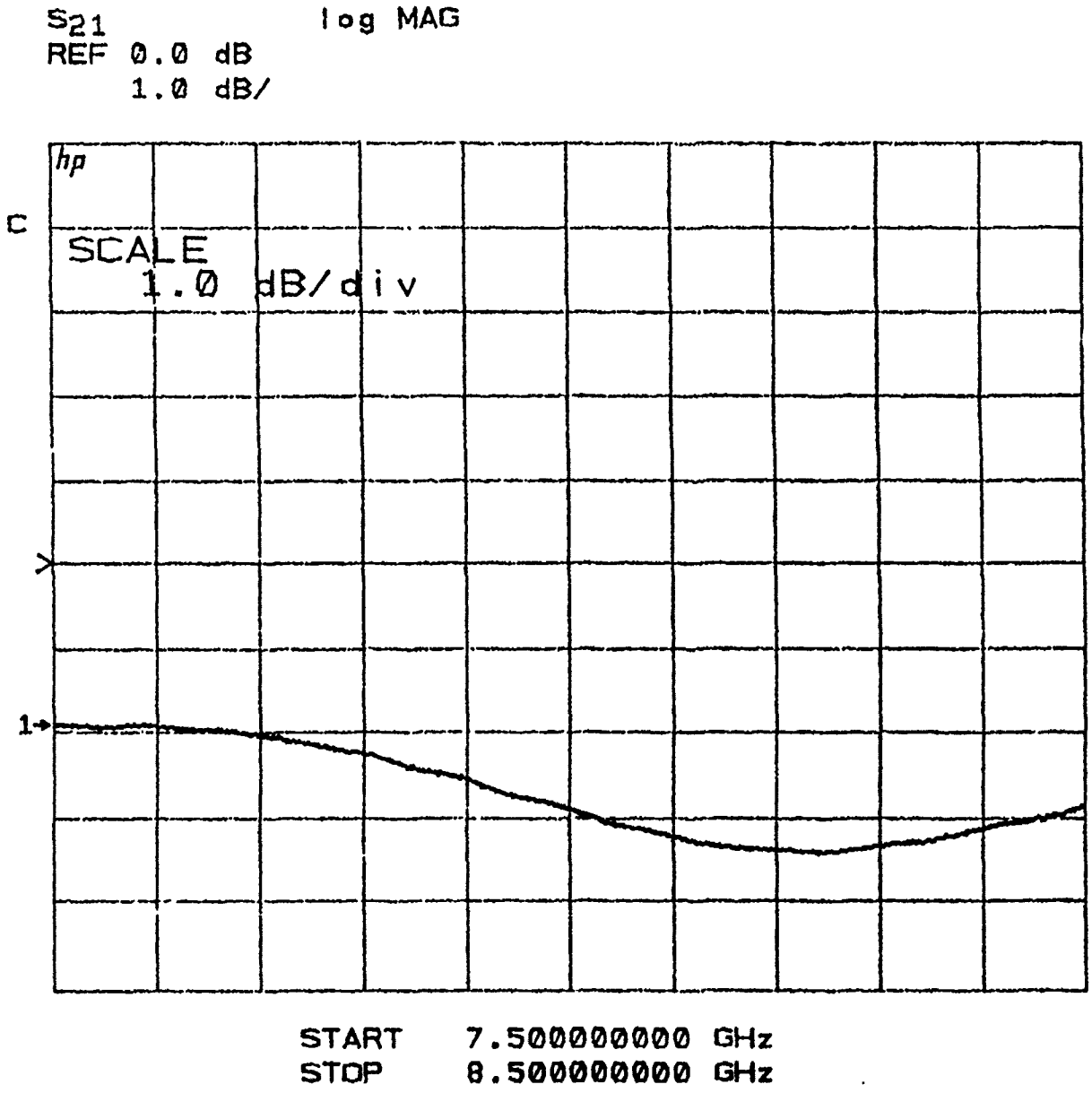

Figure A.5. Insertion Loss, SL=0.412 Inches, SW=0.01 Inches

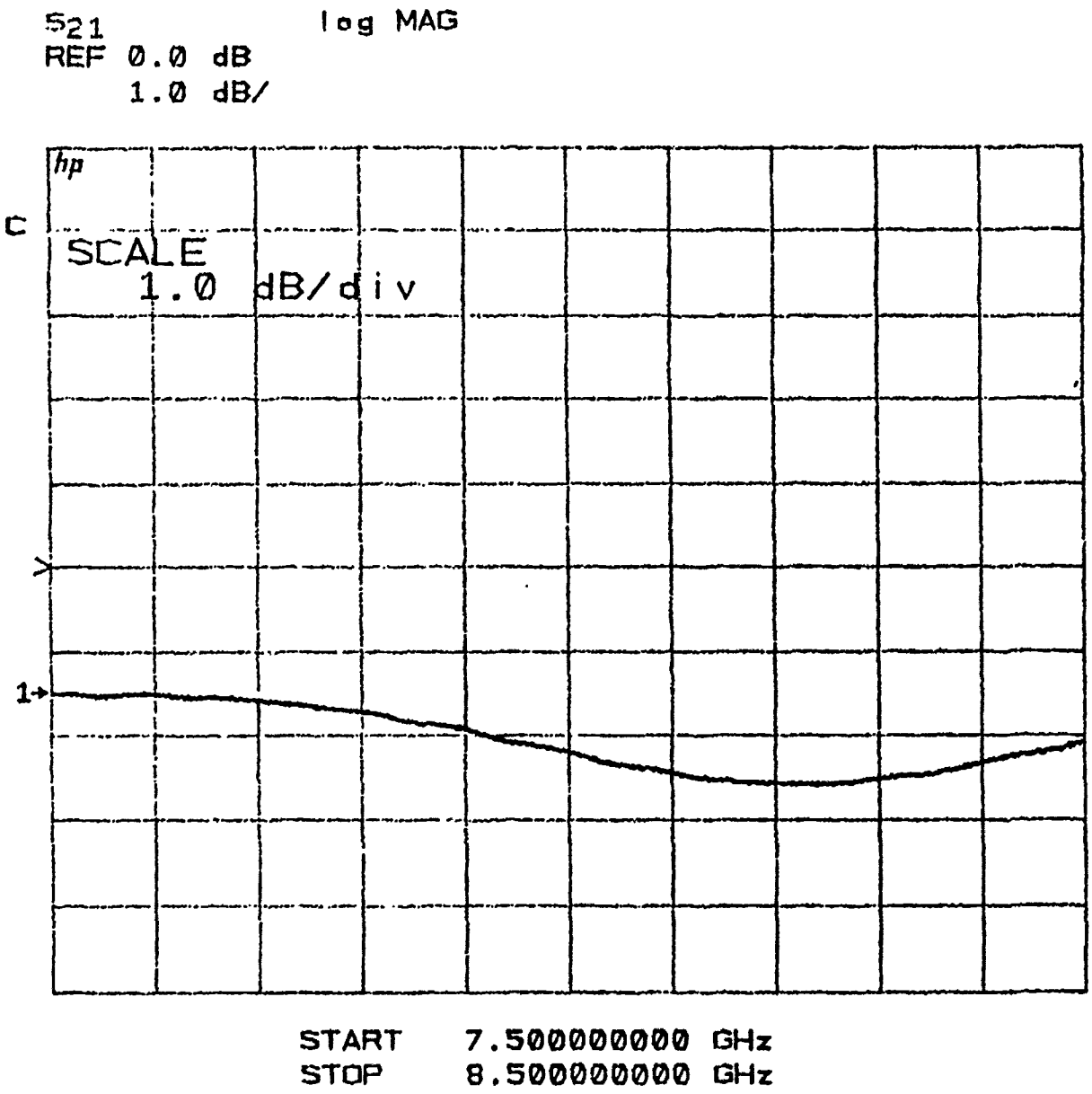

Figure A.6. Insertion Loss, SL=0.371 Inches, SW=0.01 Inches

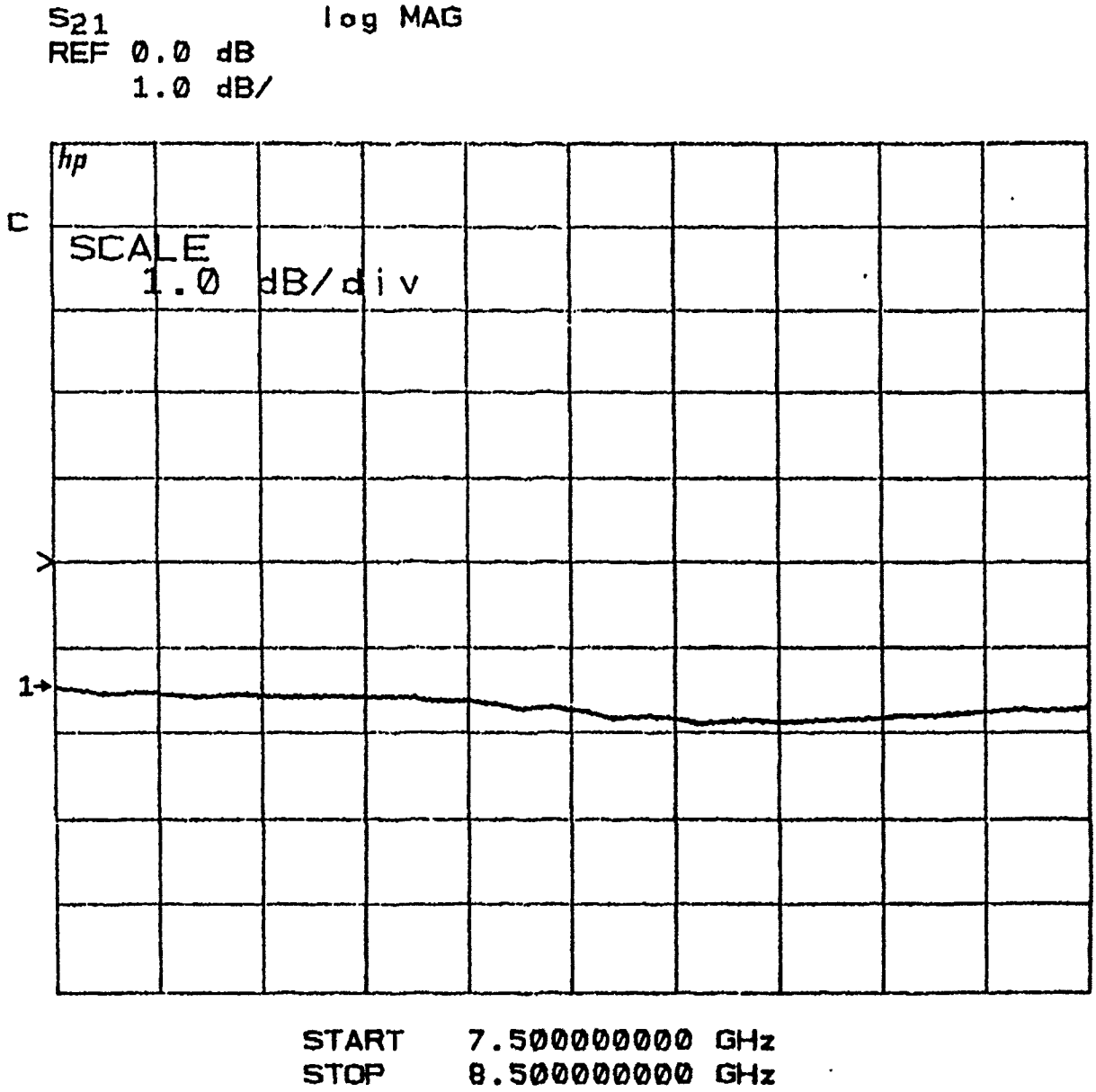

Figure A.7. Insertion Loss, SL=0.330 Inches, SW=0.01 Inches

Bibliography

1. C. J. Sletten, ed., *Reflector and Lens Antennas.* Norwood, MA: Artech House, 1988.
2. D. T. McGrath, "Slot-coupled microstrip constrained lens," in *Proc. Antenna Applications Symp*, (Champaign, IL), pp. 139–168, September 1987.
3. J. P. Montgomery, D. Runyon, and J. Fuller, "Multibeam lens antenna for EHF SATCOM," Tech. Rep. RADC-TR-88-197, Rome Air Developement Center, 1988.
4. W. E. Kock, "Metal lens antennas," *PROC. IRE*, vol. 34, pp. 828–836, November 1946.
5. D. T. McGrath, "Two-degree-of-freedom linear and planar microwave array lenses," Tech. Rep. RADC-TR-84-215, Rome Air Developement Center, 1984.
6. D. T. McGrath, "A lightweight constrained lens for wide angle scan in two planes," in *Proc. Antenna Applications Symp*, (Champaign, IL), pp. 343–365, September 1986.
7. J. B. Knorr, "Slot-line transitions," *IEEE Trans. Microwave Theory Tech.*, vol. MTT-22, pp. 548–554, 1974.
8. D. McGrath, D. Mullinix, and K. Huck, "FORTRAN subroutines for the design of printed circuit antennas," Tech. Rep. RADC-TR-86-08, Rome Air Developement Center, 1986.
9. K. Gupta, R. Garg, and I. Bahl, *Microstrip Lines and Slotlines.* Norwood, MA: Artech House, 1979.
10. J. J. Lee, "Slotline impedance," *IEEE Trans. Microwave Theory Tech.*, vol. MTT-39, pp. 666-672, 1991.
11. E. O. Hammerstad, "Equations for microstrip circuit design," in *Proc. European Microwave Conf.*, pp. 268–272, 1975.
12. J. B. Knorr and J. Saenz, "End effect in a shorted slot," *IEEE Trans. Microwave Theory Tech.*, vol. MTT-21, pp. 579–580, 1973.
13. D. A. Mullinix, "Practical considerations relative to the design and manufacture of microstrip antennas," Master's thesis, University of Lowell, Lowell, MA, 1990.
14. D. T. McGrath, "Planar three-dimensional constrained lenses," *IEEE Trans. Antennas Propagat.*, vol. AP-34, pp. 46–50, 1986.